Genome-wide association study between SARS-CoV-2 single nucleotide polymorphisms and virus copies during infections

Ke Li[1,2,#], Chrispin Chaguza[1,2], Yi Ting Chew[1,2], Nicholas F.G. Chen[1], David Ferguson[3,4], Sameer Pandya[3,4], Nick Kerantzas[3,4], Wade Schulz[3,4], Yale SARS-CoV-2 Genomic Surveillance Initiative*, Anne M. Hahn[1], Virginia E. Pitzer[1,2], Daniel M. Weinberger[1,2], Nathan D. Grubaugh[1,2,5,#]

[1] Department of Epidemiology of Microbial Diseases, Yale School of Public Health, New Haven, CT, USA
[2] Public Health Modeling Unit, Yale School of Public Health, New Haven, CT, USA
[3] Department of Laboratory Medicine, Yale School of Medicine, New Haven, CT, USA
[4] Yale Center for Genome Analysis, Yale University, New Haven, CT, USA
[5] Department of Ecology and Evolutionary Biology, Yale University, New Haven, CT, USA
* Authors listed at the end of the manuscript
[#] corresponding authors: ke.li.kl662@yale.edu; nathan.grubaugh@yale.edu

Abstract

Variations in viral loads generated during SARS-CoV-2 infections can influence COVID-19 disease progression and the likelihood of onward transmission. However, the host and virus factors that may impact viral loads and infection dynamics are not fully understood. Here, we conducted virus whole genome sequencing and measured viral copies using RT-qPCR from 9,902 SARS-CoV-2 infections over a 2-year period to examine the relative impact of host factors and virus genetic variation on changes in viral copies. We first used statistical regression models to show that host age and SARS-CoV-2 variant significantly impact viral copies, but vaccination status does not. Then, using a genome-wide association study (GWAS) approach, we identified multiple nucleotide substitutions corresponding to amino acid changes in the SARS-CoV-2 genome associated with variations in viral copies. In particular, we analyzed the temporal patterns and found that SNPs associated with higher viral copies were predominantly observed in Omicron BA.2/BA.4/BA.5/XBB infections, whereas those associated with decreased viral copies were mostly observed in infections with Delta and Omicron BA.1 variants. Our work showcases how GWAS can be a useful tool for probing phenotypes related to SNPs in viral genomes, which can be used to characterize emerging variants and monitor therapeutic interventions.

Introduction

Continued SARS-CoV-2 transmission and evolution has propelled the COVID-19 pandemic. Peak viral replication in the upper respiratory tract occurs during the first few days of infection [1]. The viral load (or copies measured by RT-qPCR) in patient samples can be used to infer the likelihood of transmission, and a strong relationship between SARS-CoV-2 transmission and viral load has been reported [2]. However, it is challenging to predict the transmission potential of SARS-CoV-2 infections using individual viral load alone, which limits our understanding of the intrinsic transmissibility of the virus at the population level [3–5]. The challenge often arises from large variations in viral load dynamic in sampled cases, which can be associated with 1) host heterogeneity, e.g., age [3] and vaccination status [6–8]; 2) distinct inherent properties of virus variants or sublineages [9], and 3) different sampling times [10]. For example, sampling during the early stages of infection may yield higher viral loads compared to later stages when viral replication has reached its peak. Nevertheless, the

relative importance of these factors influencing viral load has not been completely explored [11,12].

Genome-wide association studies (GWAS) have emerged as a useful tool in the field of genetics, providing an approach to unraveling the complex interplay between genetic variations and observable traits, including diseases and drug resistance, as reviewed in [13]. Through testing hundreds of thousands of genetic variants across many genomes, GWAS analysis enables us to identify specific mutations or genes in humans that contribute significantly to observed phenotypic variations, such as HIV1-load [14]. Several studies have employed GWAS analysis to identify and investigate the association between human genetic variations across different individuals and the severity of COVID-19, shedding light on genetic variations that are related to severe infections [15–17]. Although GWAS was originally developed for humans, recently, it's been increasingly adapted and applied to study the genetic basis of several microbial traits [18], especially for bacteria. Although there are studies utilizing a GWAS method to validate the association between the viral genome and HIV drug resistance [19], and to study the effect of human immunity on hepatitis C virus [20], the application of GWAS analysis to study viral genomes and examine the association between viral mutations and related phenotypes is limited. The confluence of the extensive existing research on SARS-CoV-2 mutations and the millions of infections that have been sequenced provides us the opportunity to evaluate the application of GWAS for viral genomics. The hypothesis-free approach has the potential to enhance our understanding of genetic determinants influencing viral fitness and evolution and further inform effective public health strategies aimed at mitigating the spread and impact of SARS-CoV-2.

In this work, we aim to investigate the relative impact of host factors and intrinsic viral genetic mutations (single nucleotide polymorphisms, SNPs) on the changes in viral copies. For this, we apply a viral GWAS analysis to SARS-CoV-2 genomic sequencing and standardized RT-qPCR data collected from the Yale New Haven Hospital from February 2021 to March 2023. Further, the availability of the whole genome sequencing data on SARS-CoV-2 infections with the relevant laboratory and patient metadata allows the identification of the association between viral mutations and viral copies for different variants of concern (VOCs). We then examine the temporal pattern of identified mutations by constructing a phylogenetic tree, drawing upon subsamples, and analyzing the time series of the fraction of mutations occurring in the sequences. Finally, we compare whether the temporal pattern is consistent across different gene segments. This multifaceted analysis contributes to unraveling the complex dynamics of SARS-CoV-2 infections, providing valuable insights into the underlying viral mutations that influence viral copies in different VOCs.

Results

Viral copies vary in SARS-CoV-2 infections

To better understand how SARS-CoV-2 viral load varies in infected individuals, we analyzed the viral copy data, along with associated host metadata (i.e., age and vaccination status), and genome sequencing data from a cohort of patients tested at the Yale New Haven Hospital (YNHH) located in Connecticut, US. We selected 9902 whole genome sequences with available viral copy data generated from remnant SARS-CoV-2 diagnostic samples over a 2-year period, from 03-Feb-2021 to 21-Mar-2023 (**Fig. 1A).** The VOCs that we identified in

our dataset during the sampling period included Alpha (n = 809), Delta (n = 1278), Gamma (n = 36), BA.1 (n = 1818), BA.2 (n = 2432), BA.4 (n = 293), BA.5 (n = 1992), XBB (n = 698), and the pre-VOC variant (named 'Other', n = 546). We conducted RT-qPCR using a standardized assay targeting the nucleocapsid (CDC 'N1' primers) for each sample to allow for cross-sample comparisons [21], except for a period during October 2021 when the PCR data were not generated. Across all samples, the viral copies, expressed as $\log_{10}$(viral copies per milliliter (Genome Equivalents/ml)), exhibited variations, ranging from 3.60 to 10.55, with a median value of 7.26 (**Fig. 1B**). The variations in viral copies could be attributed either to the introduction and/or replacement of different VOCs, each with its own epidemic curve, or to the stochasticity from the sampling process. To reduce stochastic effects, we aggregated the viral copies by month and still observed large variations in the viral copies across the months (**Fig. 1C**). Notably, we observed the lowest median value of viral copies (median = 6.49) in February 2022, during which 96.3% of the sampled sequences tested positive for BA.1 infections. By contrast, we observed the highest median value of viral copies (median = 7.70) in June 2022, during which the sampled sequences tested positive for BA.2 (64.9%), BA.4 (6%), or BA.5 (29.1%) infections. Taken together, we showed a wide range of viral copies in the sampled SARS-CoV-2 infections with different VOCs, utilizing data from genomic surveillance and standardized RT-qPCR tests.

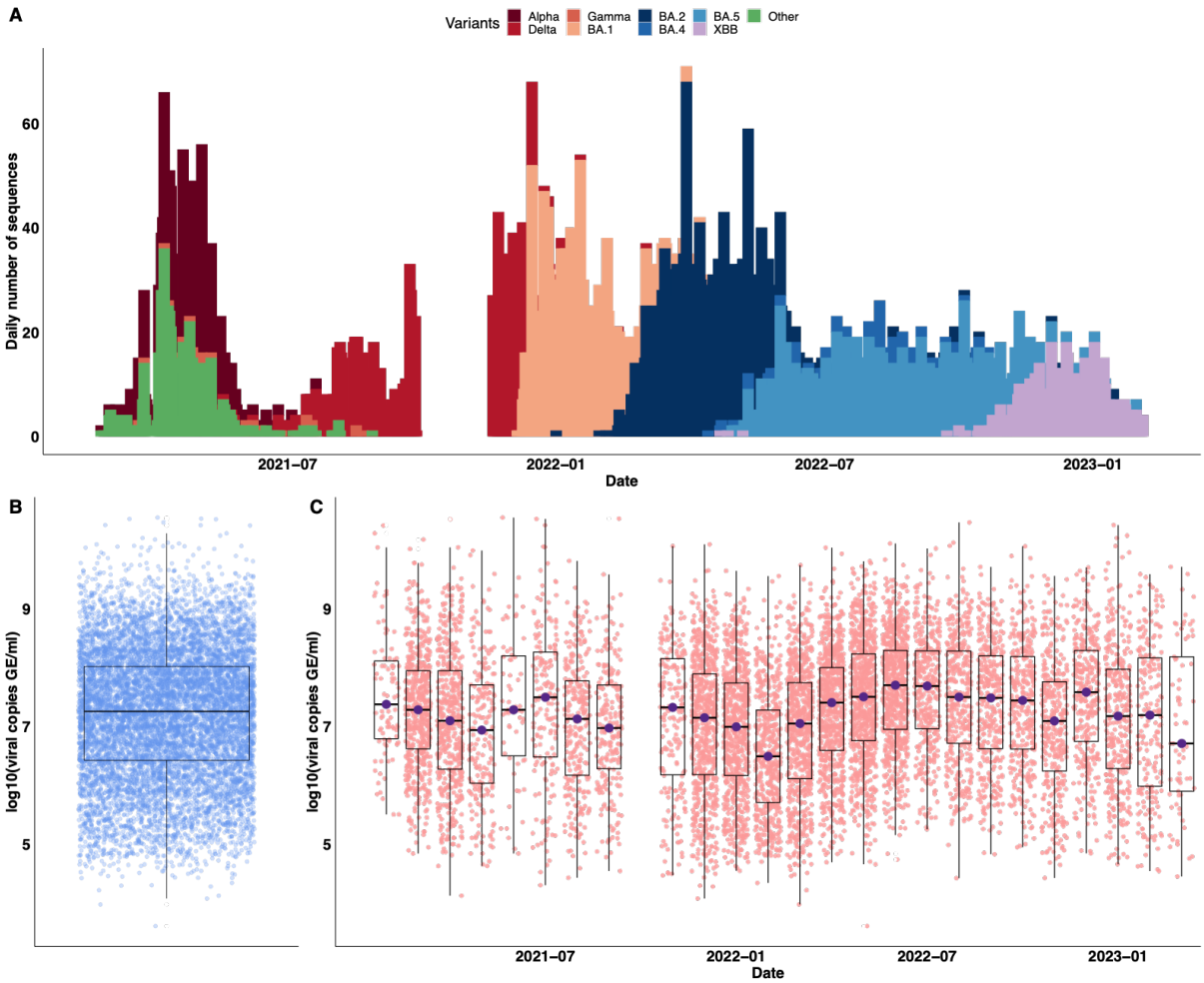

Figure 1. Genomic sequences of SARS-CoV-2 infections and associated viral copies from cross-sectional samples collected in Connecticut, US. (**A**) The daily number of genomic sequences of SARS-CoV-2 VOCs from February 2021 to March 2023. (**B**) The summary of viral copies of all samples, expressed as log_{10}(viral copies per milliliter). (**C**) The summary of viral copies aggregated by month.

The data gap in October 2021 is because we were unable to conduct PCR to obtain viral copies during this time.

Viral copies correlate with age and variants, but not with vaccination status

Having uncovered a large variability in the observed viral copies from the samples, we next assessed whether host factors, such as age and vaccination status, or inherent differences among VOCs contribute to changes in viral copies. To do this, we first summarized and compared viral copies in various age groups (**Fig. 2A**). A positive correlation has been previously reported between age and SARS-CoV-2 viral copies, showing that younger age groups had lower viral copies independent of gender and/or symptom duration [22]. We observed a similar result in our dataset and found that the older age group (i.e., >70 years old) had the highest viral copies compared with other age groups (mean = 7.47, 95% confidence interval (CI): [5.12, 9.49], $p < 0.001$, Wilcoxon signed-rank test). For the effect of vaccination on viral copies, some studies have demonstrated that although vaccination reduced the risk of infections with the Delta variant, no significant difference in peak viral copies was found between fully vaccinated and unvaccinated individuals [6,7,23]. In contrast, other studies have shown that vaccination reduced viral copies in BA.1 infections among boosted individuals compared to unvaccinated ones [8]. These results suggest the effect of vaccination on viral copies may depend on the characteristics of the infecting SARS-CoV-2 variant. We compared viral copies among groups with different vaccination statuses to assess the impact of vaccination on viral copies (**Fig. 2B**), and no statistically significant differences were detected between the groups in our data ($p > 0.05$, Wilcoxon signed-rank test). Finally, we compared viral copies stratified by variant category (**Fig. 2C**). Combining samples collected from all age and vaccination status groups for each variant, we found that the overall mean values of viral copies were lowest for infections with BA.1 (mean = 6.83, 95% CI: [4.87, 8.87], $p < 0.001$, Wilcoxon signed-rank test) compared to infections with other variants.

Since several factors may simultaneously impact the SARS-CoV-2 viral load, next, we sought to quantify the combined impact of age, vaccination status, and VOCs on the observed viral copies. To achieve this, we fitted a multivariate linear regression model, with viral copies as the outcome variable and age, vaccination, and VOCs as covariates (**Fig. 2D**). We found that the older age group (i.e., age >70 years old) had a positive association with viral copies (mean = 0.17, 95% CI: [0.09, 0.25], $p < 0.001$) compared with the reference group (i.e., age <18 years old). We also found that vaccination status was not associated with viral copies (i.e., 95% CIs of the vaccination coefficients span 0, $p > 0.05$). Notably, we showed that infections with BA.1 were associated with reduced viral copies, with a mean effect size of -0.34 (95% CI: [-0.44, -0.24], $p < 0.001$) in the same age group and vaccination status, compared to the Other variant. We also showed that infections with BA.2 (mean = 0.19, 95% CI: [0.09, 0.28], $p < 0.001$), BA.4, or BA.5 (mean = 0.17, 95% CI: [0.07, 0.26], $p < 0.001$) were associated with increased viral copies. Among them, infections with BA.4 were associated with the largest positive effect size (mean = 0.27, 95% CI: [0.12, 0.41], $p < 0.001$). Our findings demonstrated that variations in viral copies were associated with infections caused by different SARS-CoV-2 variants and the older age group. This implies that intrinsic factors of the viruses, such as genetic mutations among distinct VOCs, are key determinants impacting viral copies.

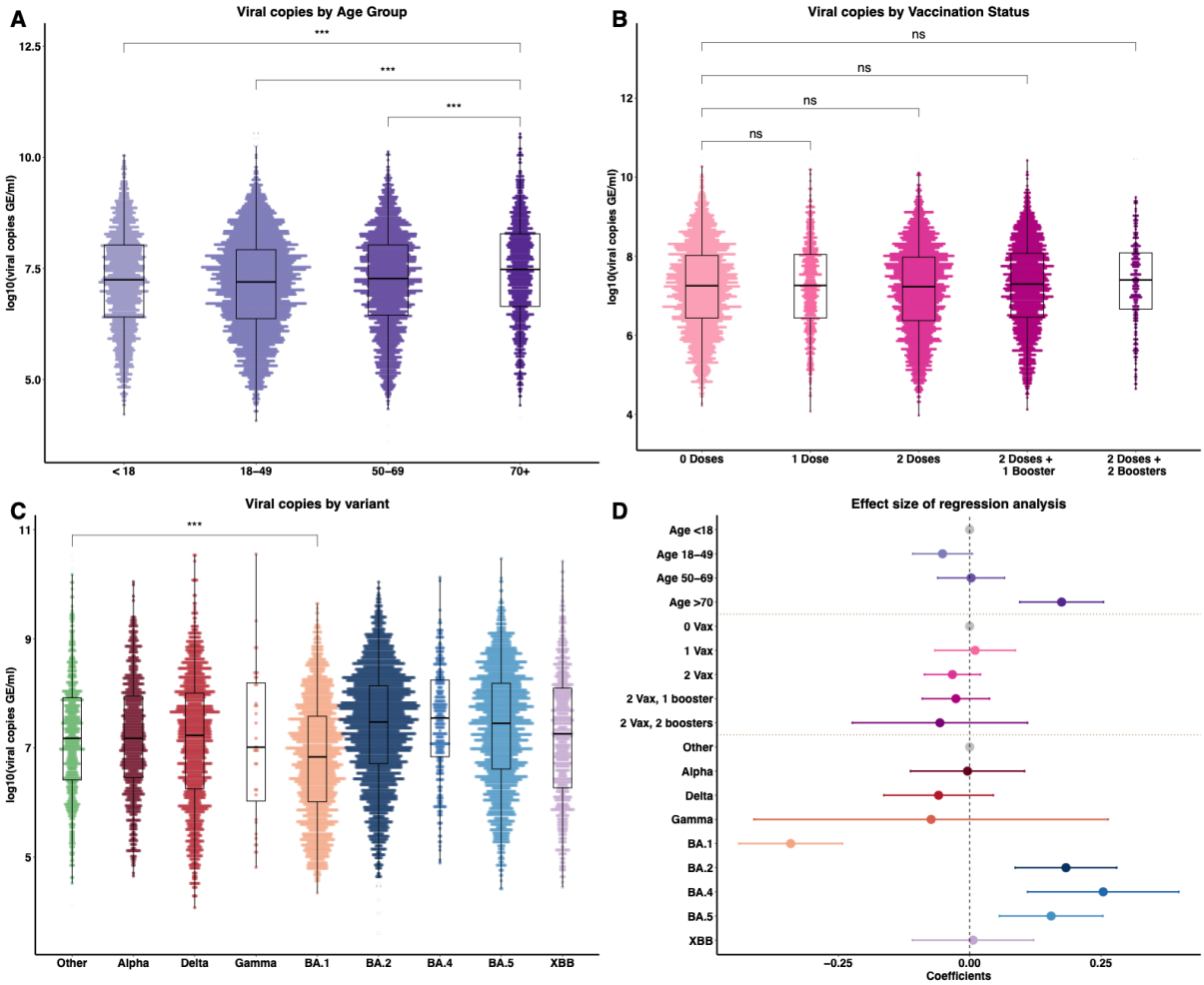

Figure 2. Viral copies by category and regression analysis results. Comparison of viral copies stratified by (**A**) age groups, (**B**) vaccination statuses, (**C**) variant of concerns. (**D**) Association of age, vaccination status, and VOCs with viral copies, expressed as log_{10}(viral copies per milliliter (Genome Equivalents/ml)). The reference groups (in gray) are Age <18 years old, 0 doses of vaccination, and the Other variant, respectively. The positive coefficients indicate the covariate is associated with higher viral copies value compared to the reference group, and vice versa. 0 Vax, 1 Vax, 2 Vax, 2 Vax 1 booster, and 2 vax 2 boosters denote vaccination statuses of 0 doses, 1 dose, 2 doses, 2 doses, and 1 booster, and 2 doses and 2 boosters, respectively, corresponding to the labels in (**B**). Results are shown as means with 95% confidence intervals. *** $p < 0.001$.

Viral GWAS reveals SARS-CoV-2 SNPs associated with viral copies

Having demonstrated that changes in SARS-CoV-2 viral copies are associated with infections caused by different viral variants or strains, especially Omicron BA.1/BA.2/BA.4/BA.5 variants (**Fig. 2D**), we then sought to identify potential genetic mutations—specifically, SNPs—that contributed to these changes in viral copies. For this, we performed a GWAS analysis using high-quality genome sequences (i.e., genome coverage > 95%). We conducted whole-genome sequencing on the 9902 SARS-CoV-2 positive specimens collected from February 2021 to March 2023. Firstly, using Wuhan-Hu-1 (GenBank MN908937.3) as the reference genome, we identified 10,697 SNPs for further testing associated with viral copies as covariates. We then checked for the population structure of the 9902 genome sequences using a multidimensional scaling (MDS) method [24] (**Fig. S1**). We observed that Delta was an outgroup to other pre-Omicron variants (i.e., pre-VOC variant (Other), Alpha, and Gamma), and BA.1 was an outgroup to the BA.2/BA.4/BA.5/XBB cluster. We included the inferred MDS

components from the pairwise SNP distance matrix of SARS-CoV-2 sequences in our model to capture the viral population structure. We also calculated the proportion of variance in our original sequence data accounted for by the MDS results. We found that 95% of the SARS-CoV-2 genetic variance could be explained by the two dimensions computed by MDS, which suggested that including these two dimensions in the regression analysis could adequately adjust for the population structure of the viral strains. The host factors, including age group and vaccination status, were also included in our model as covariates.

Using the multivariate linear regression model on viral copies for each SNP, we identified 113 SNPs exceeding the permuted threshold for genome-wide significance ($p = 4.67 \times 10^{-6}$, dashed line, **Fig. 3A**). The threshold value was calculated as 0.05 divided by 10,697 SNPs [25]. We found that the observed distribution of *p*-values closely matches the expected distribution under the null hypothesis of no association (**Fig. S2A**). To ascertain whether those SNPs have a negative or positive impact on viral copies and evaluate their effect size, we extracted the coefficients (β) of the SNPs with $p < 1 \times 10^{-10}$ and their standard errors (σ) from the regression model (dashed box, **Fig. 3B**). We then annotated the SNPs to identify the associated amino acids, and among them, 44 SNPs were non-synonymous (i.e., changed the amino acid; **Fig. 3C**). We found that a non-synonymous change G252V, located on the S gene, had the most significant association with increased viral copies ($p = 5.60 \times 10^{-22}$, β = 1.21, σ = 0.12). By contrast, the amino acid change most strongly associated with a negative effect on viral copies was ORF1ab:V2857A ($p = 5.66 \times 10^{-11}$, β = -1.32, σ = 0.20).

To assess the impact of adjusting for the population structure of the SARS-CoV-2 strains using the MDS components on the regression results, we conducted a sensitivity analysis on the genome sequences using the defined sequence clusters (a categorical variable) as covariates. Clusters were defined using a *k*-means clustering method (**Fig. S1**). By doing this, we identified only 31 SNPs exceeding the permuted threshold (**Fig. S3**), compared to 113 SNPs found in the analysis using MDS-computed dimensions as population control. The observed distribution of *p*-values also closely matched the expected distribution under the null hypothesis of no association (**Fig. S2B**). Of these, 25 out of the 31 identified amino acid changes were consistent with those previously observed, except for ORF1ab:P3395H, S:Q498R, N679K, Q954H, N969K, and N:R203M. The results may be more likely to reflect the SNPs that influence the viral copies independent of lineage.

We also examined the association between viral copies and SNPs after adjusting for the population structure based on the VOCs themselves, which broadly correspond to the identified sequence clusters. To do this, we conducted sensitivity analyses on the genome sequences within each sequence cluster defined by a *k*-means clustering method (**Fig. S1**). We showed that only a few SNPs were found (**Figs. S4-7**), mostly within the Omicron BA.2/BA.4/BA.5/XBB cluster (**Fig. S7**).

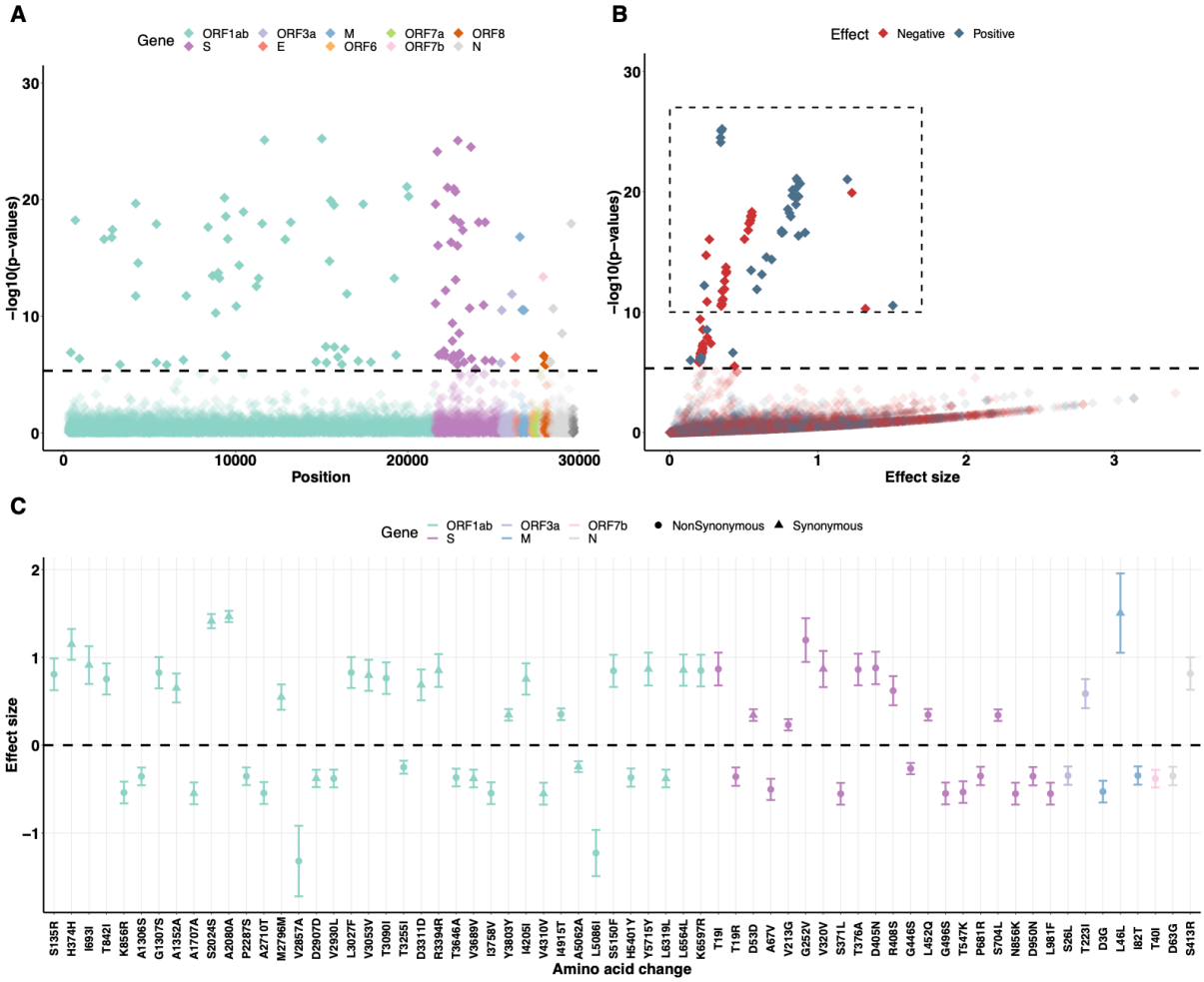

Figure 3. GWAS analysis identifies several single nucleotide polymorphisms (SNPs) that are associated with the changes in viral copies. (**A**) Genome-wide association results of the impact of identified SNPs on viral copies during SARS-CoV-2 infection. The dashed line indicates the permuted threshold for genome-wide significance $p = 4.67 \times 10^{-6}$. Significant SNPs are shown with solid colors. (**B**) SNPs (with $p < 1 \times 10^{-10}$) that have positive (blue) or negative (red) effects on viral copies. (**C**) The corresponding synonymous (triangles) and non-synonymous (circles) amino acid changes that associate with increased or decreased viral copies. Data is shown as means with 95% confidence intervals. The estimated effective sizes and associated standard deviations are given in **Table S1**. A Q-Q plot showing the observed distribution of *p*-value and the expected distribution is given in **Fig. S2**.

The impact of amino acid changes in the S gene on viral copies is dependent on the variant

Having identified the 44 non-synonymous SNPs with statistically significant effects on viral copies in our primary analysis, we next sought to understand the temporal patterns of the emergence of these amino acid changes (**Fig. 4**). To investigate the clustering of these SNPs, we randomly sampled approximately 120 genome sequences from each VOC category (only 36 sequences were available for Gamma in our dataset) and generated a phylogenetic tree drawing upon the subsamples (**Fig. 4A**). We first focused on the 18 amino acid changes in the S gene and found a clear pattern in how these mutations emerged by VOC (**Fig. 4A** heatmap). Notably, we found that all amino acid changes associated with a positive effect on viral copies were found in BA.2/BA.4/BA.5/XBB infections. Often, more than one amino acid

change was observed in each sampled sequence, suggesting genetic linkage between these SNPs. In particular, we identified that the amino acid changes L452Q ($p = 3.91 \times 10^{-25}$, β = 0.34, σ = 0.03) and S704L ($p = 1.35 \times 10^{-24}$, β = 0.34, σ = 0.03) associated with a positive effect on viral copies were typically observed in combination with BA.2 infections—specifically, lineage BA.2.12.1. By contrast, a retrospective cohort study has shown that the risk of death due to COVID-19 was lower for Omicron BA.1 compared with Delta (B.1.617.2) infections [26]. Here, we observed that the amino acid changes with negative effects on viral copies were mostly associated with BA.1 and Delta infections. Among these SNPs, we observed that A67V, S371P, G496S, T547K, N856K, and L981F, exclusively associated with BA.1 infections, had a comparatively larger (negative) impact on viral copies (mean = -0.54, 95% CI: [-0.55, -0.51]) than the others (T19R, G446S, P681R and D950N) with a mean of -0.33 and a 95% CI: [-0.36, -0.27], which were also present in Delta or XBB infections.

To explore the temporal dynamics of these S gene amino acid changes, we calculated the fraction of mutations occurring in the sequences for each day, thereby accounting for the number of introductions to the population (**Fig. 4B**). We observed SNPs (T19I, V213G, T376A, D405N, and R408S) with a positive impact on viral copies emerging in sequences sampled from February 2022, when BA.2 was first detected in Connecticut. These SNPs were consistently observed in almost every sequence thereafter. By contrast, we found that the other two amino acid changes (L452Q and S704L) that had a positive effect on viral copies were only in the samples from BA.2 infections and did not arise again in lineages of BA.4 or BA.5. The G252V amino acid change was associated with higher viral copies; however, we found that the SNP only appeared in a few sequences associated with XBB infections. For those SNPs that had a negative association with viral copies, we observed that most of them (A67V, S371P, G496S, T547K, N856K, and L981F) were present in samples associated with BA.1 infections and did not persist when BA.1 was replaced by BA.2. We also noted that other mutations, e.g., T19R, P681R and D950N, were only found in samples from Delta infections, and that G446S ($p = 5.56 \times 10^{-16}$, β = -0.26, σ = 0.03) was first found in samples from BA.1 infections but absent in BA.2/BA.4/BA.5 infections and reemerged in XBB infections.

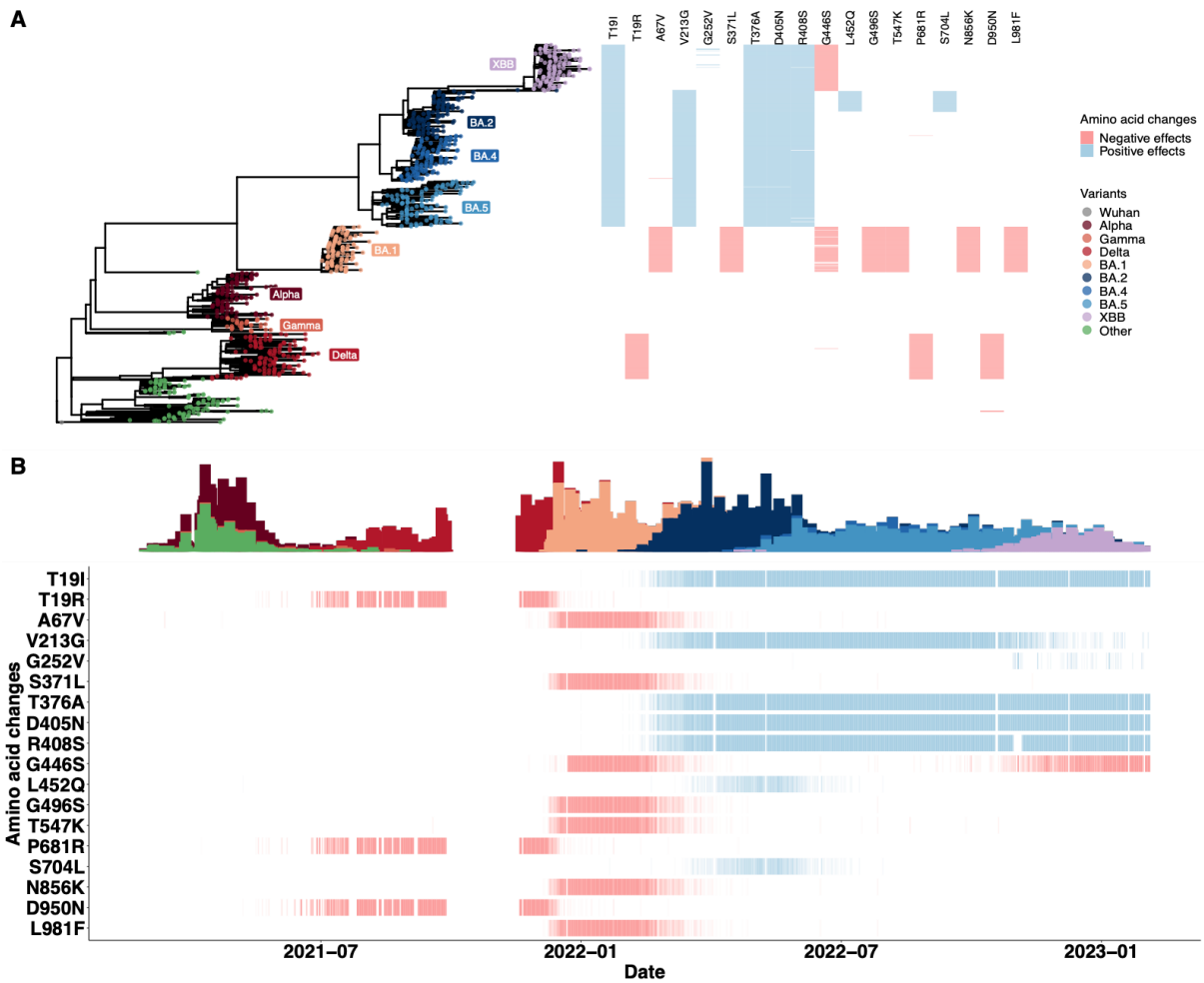

Figure 4. The temporal dynamics of amino acid changes in the S gene associated with changes in viral copies. The results are based on the multivariate regression analysis using the two MDS components as covariates. (**A**) The phylogenetic tree estimated from a representative set of 996 genome sequences showing variant assignments and the locations of amino acid changes that increase (blue) or decrease (red) viral copies. (**B**) The temporal dynamics of the SNPs from February 2021 to March 2023. The transparency of the color corresponds to the mutation fraction in the daily sequence count: transparent color indicates low fractions, and opaque color indicates high fractions.

Amino acid changes in the ORF1ab gene show similar temporal patterns to those in the S gene

Having observed the SNP pattern in the S gene, our next aim was to determine if the same temporal patterns persisted for the amino acid changes in the ORF1ab gene (**Fig. 5**). We found that the presence of SNPs associated with an increase in viral copies were observed in BA.2/BA.4/BA.5/XBB infections, while those associated with a decrease in viral copies were observed in Delta or BA.1 infections (**Fig. 5A**). This pattern was consistent with our observations for the S gene. Additionally, we identified similar temporal dynamics of mutations in the ORF1ab gene, mirroring the pattern seen in the S gene (**Fig. 5B**). These trends were consistently observed in the temporal dynamics of amino acid changes in the M, ORF3a, and ORF7b genes as well (**Fig. S8**). In particular, we found that ORF1ab:I4915T (p = 2.36×10^{-25}, β = 0.35, σ = 0.04) was only associated with BA. 2 infections. We also found that, although ORF1ab:V2857A had the most significant effect in reducing viral copies (p = 5.66×10^{-11}, β = -1.32, σ = 0.20), it only appeared in 24 samples (0.24% of the sample size)

with BA.1 infections. Furthermore, we identified that ORF1ab:T3255I ($p = 1.02 \times 10^{-11}$, β = -0.25, σ = 0.04) was consistently detected in Delta and other Omicron variants and was associated with decreased viral copies.

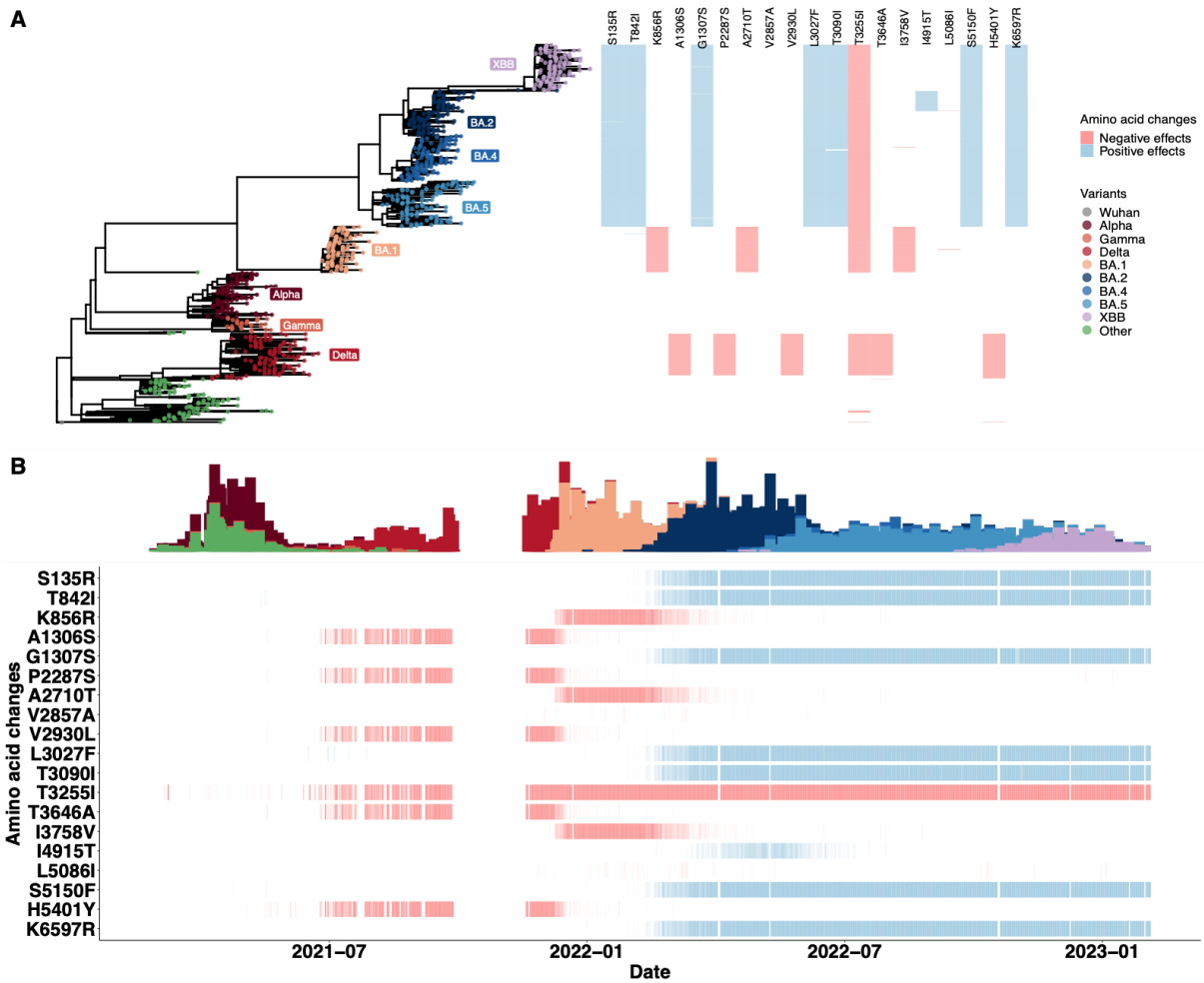

Figure 5. **The temporal dynamics of amino acid changes in the ORF1ab gene associated with changes in viral copies.** The results are based on the multivariate regression analysis using the two MDS components as covariates. (**A**) The phylogenetic tree estimated from a representative set of 996 genome sequences showing variant assignments and the locations of amino acid changes that increase (blue) or decrease (red) viral copies. (**B**) The temporal dynamics of the SNPs from February 2021 to March 2023. The transparency of the color corresponds to the mutation fraction in the daily sequence count: transparent color indicates low fractions, and opaque color indicates high fractions.

GWAS analysis identified a subset of variant-defining amino acid substitutions

Experimental investigations on the specific amino acid substitutions that define emerging VOCs for SARS-CoV-2 have yielded insights into viral transmissibility and immune escape [27–33]. Here, we compared the identified SNPs using our GWAS method with all variant-defining amino acid changes (**Fig. 6**). The variant-defining amino acid changes were defined as those mutations with >75% prevalence in at least one lineage, as estimated on the outbreak.info website [33]. Our GWAS analysis identified a subset of the variant-defining amino acid substitutions in the S (**Fig. 6A**) and ORF1ab genes (**Fig. 6B**) that were associated with the changes in viral copies. More importantly, we were able to identify S L452Q and

S704L, which primarily emerged within the sublineage BA.2.12.1. These were not identified as variant-defining mutations on the outbreak.info website. The results imply the applicability of GWAS of SARS-CoV-2 genome sequences to identify the associations between viral copies and amino acid changes without exclusively focusing on variant-defining SNPs.

Figure 6. Comparison of key variant-defining amino acid changes with GWAS-identified substitutions. The comparison of the key amino acid changes (dark purple) in each variant, with GWAS-identified SNPs that were associated with negative (red) or positive (blue) effects on viral copies in the (**A**) S gene and (**B**) ORF1ab gene. The results of GWAS analysis using the two dimensions computed by MDS as covariates are shown as "GWAS 1", and the results of GWAS analysis using the categorical clusters as covariates are shown as "GWAS 2". The effective sizes of identified SNPs using different population control methods are given in **Tables S1** and **S2**, respectively.

Discussion

We conducted a GWAS analysis on 9,902 high-quality SARS-CoV-2 genome sequences generated from two years of genomic surveillance in Connecticut, US to identify and evaluate SNPs that were associated with variations in viral copies during infections. Both viral factors and host characteristics can have impacts on viral replication at the within-host level [3,6–9]. Using a GWAS approach, we were able to identify and examine virus-related factors that

were associated with the observed variations in viral copies. This was achieved by combining data from a large cohort of individuals infected with different VOCs and employing a regression model that accounted for both individual (i.e., age and vaccination status) and virus-level factors (i.e., specific SNPs and genetic background) in viral copies. We identified several SNPs corresponding to non-synonymous amino acid changes in the SARS-CoV-2 genome that were individually associated with the variations in viral copies. In particular, temporal patterns of the SNPs revealed that SNPs associated with increased viral copies were predominantly observed in Omicron BA.2/BA.4/BA.5/XBB infections, whereas those associated with decreased viral copies were mostly observed in infections with Delta and Omicron BA.1 variants.

Using GWAS analysis, we identified a subset of variant-defining amino acid changes in Delta and Omicron variants. Note that we did not detect any substitutions in the Alpha and Gamma variants (likely due to the low sample size for Gamma). We also identified SNPs that did not define any major variant category, including S:L452Q and S704L that were specifically associated with BA.2.12.1, a sublineage of BA.2 that briefly dominated during the pandemic (i.e., dominated mainly in the US between March and May 2022). This highlights the application of GWAS for identifying SNPs associated with important phenotypic effects without requiring a set of lineage-defining mutations to be defined a priori. Nevertheless, there are several reasons why we only detected a subset of the SNPs that defined different VOCs. Firstly, SNPs with small effect sizes may not be detected due to the stringent statistical significance thresholds applied in GWAS. Secondly, lineage-defining SNPs that are in low linkage disequilibrium with the causal mutations may not be detected [34], even if they may be functionally relevant. Our results showcase how GWAS can help to narrow the focus of SNPs associated with specific phenotypes, generating hypotheses for further investigation.

A key result from our analysis is that SNPs associated with viral copies did not exhibit the same temporal dynamics, even though they could have similar (either positive or negative) effects on viral copies. Some amino acid changes, for example, ORF1ab:I4915T (positive effects), were only present in samples with BA.2 infections and disappeared when new Omicron variants emerged. Other SNPs (e.g., S:T19R and ORF1ab:S135R), while also associated with higher viral copies, were observed and persisted in all BA.2/BA.4/BA.5/XBB infections. The distinct temporal pattern of SNPs, dependent on VOCs, may help explain the different fitness levels (e.g., intrinsic transmissibility or immune escape) of each variant [35,36]. For example, S:L452Q has been suggested to increase viral infectivity and affinity to angiotensin-converting enzyme 2, thereby enhancing the ability to circumvent vaccine-induced immune responses [37]. Different VOCs have been suggested to exhibit variations in cell tropisms, with BA.1 showing a preference for the upper respiratory tract [1,38]. This preference could be associated with specific mutations which may have causal effects on intracellular viral replication dynamics in different host cell types. Recent studies indicated that BA.2 infections were characterized by a higher peak viral load, as shown in [39–41]. This is consistent with our analysis, where we found that SNPs associated with an increase in viral copies were linked to BA.2 infections. The shift from negative to positive effect SNPs on viral copies from BA.1 to BA.2 may explain the observed rapid replacement of BA.1 by BA.2 and the subsequent fast spread of BA.2 infections [42].

In addition, we showed that S:G446S was associated with decreased viral copies in primarily BA.1 and XBB infections. Motozono et al. [43] have previously demonstrated that the mutation could affect antigen presentation and potentiate antiviral activity by vaccine-induced T cells, leading to enhanced T cell recognition. We also identified a previously

392 studied amino acid change, T3255I, in the ORF1ab gene. This SNP is located at site 492 in
393 non-structural protein 4 (NSP4) and carried by both the Delta and Omicron variants. The
394 mutation has been implied to increase the replication capacity of the virus and improve its
395 ability to evade host immune responses [44]. Using phylogenomic analysis, we identified that
396 the mutation was present in both the Delta and Omicron variants, with a negative impact on
397 viral copies. These two mutations, S:G446S and ORF1ab:T3255I were found in different
398 genetic backgrounds, which may provide evidence that they may influence the viral load
399 independent of the background/lineage.
400
401 Several studies indicate that the Delta variant is linked to higher viral loads and increased
402 transmissibility compared to the Alpha variant [45–47]. In contrast, another study found no
403 significant difference in the mean peak viral load (indicated by a cycle threshold value)
404 between Delta infections and the pre-VOC variant [7,48]. Here, we identified mostly SNPs
405 associated with decreased viral copies in Delta infections, except for one N:R203M (**Fig. S9**).
406 The discrepancy of these results suggests that the relationship between Delta variant
407 infections, viral copies, and associated factors is multifaceted, requiring careful consideration
408 of several factors and large datasets to investigate such patterns. Differences in population
409 demographics, the dynamic nature of viral evolution, or study methodologies (e.g., diagnostic
410 assays) could all influence the observed viral copies. Previous studies inferring viral load
411 differences in infections by VOCs normally analyzed viral copy data from large cohorts of
412 individuals without explicitly accounting for the influence of host factors, such as age, host
413 immunity, symptomatic conditions, and infection history. These factors could potentially
414 contribute to variations in viral load. Not only does host immunity and variants shape within-
415 host viral dynamics of SARS-CoV-2 infections, but individual heterogeneity also plays a more
416 important role in determining the viral kinetics [49]. For instance, an increased viral load was
417 observed primarily in the younger population with Delta infections [46]. The association of
418 higher viral loads with a younger age group raises intriguing questions about age-related
419 susceptibility and immune responses, both for specific variants and for SARS-CoV-2 in
420 general, as discussed in [50]. Alternatively, inconsistent results in various studies may arise
421 from using data on different sub-lineages of SARS-CoV-2, for example those belonging to
422 the Delta variant (e.g., B.1.617.2 and AY). Another possibility for not detecting any positive-
423 effect SNPs in Delta infections is that the increased viral copies in Delta infections may result
424 from the concurrent accumulation of multiple mutations, which may introduce non-additive
425 epistatic effects that can be difficult to unpick [28]. In this study, however, we employed a
426 series of single SNP regression models to identify the underlying SNPs associated with the
427 changes in viral copies. This was achieved by performing individual regression analyses for
428 each of the 10,697 SNPs one at a time, without accounting for potential interactions between
429 SNPs. A multiple SNP regression study, which allows for testing potential interactions or joint
430 effects among multiple SNPs, albeit challenging due to multicollinearity, will be left for future
431 study.
432
433 There are limitations to our study. First, the common cooccurrences of identified SNPs make
434 it impossible to evaluate their individual effects on viral copies, which is an overall limitation
435 of GWAS. However, our findings provide valuable insights into the overall genetic landscape
436 of the viral population and identify potential genetic variants that could be further explored.
437 Second, we assumed that the distribution of times between infection and sample collection
438 was similar through time and across variants as these data were not available. Given our
439 samples were taken frequently over a 2-year period, we do not anticipate that this assumption
440 will qualitatively impact our results. Third, our study primarily focuses on the genetic variants
441 in VOCs, neglecting other factors such as host immune responses or environmental

influences, partially captured by the host-associated covariates, including age and vaccination status in this study, that may also contribute to the changes in viral copies. Further study will be needed to address the impact of these factors on viral copies, for example, genome-to-genome analysis to reveal the impact of host-viral genetic interactions in SARS-CoV-2 infections [20,51]. Fourth, our data were obtained from a specific geographic region, whose population diversity may not necessarily be similar to other settings; therefore, extrapolating these findings to a broader population may require caution. Additionally, focusing solely on consensus genomic changes in the analysis could overlook the genetic diversity within the sample, which may also influence variations in viral load. Despite these constraints, our study highlights the importance of sustained genomic surveillance and the need for comprehensive analyses to understand the nuanced impact of specific genetic variations on viral copies at the within-host level, and its implications for viral transmissibility and immune escape at the population level. Further work and collaborative efforts are essential to elucidate the complex interplay between viral genetics, host factors, and the dynamics of transmission associated with emerging variants. Such studies could inform predictive early warning public health systems regarding the emergence of potentially highly transmissible viral strains based on their constellation of mutations.

Recently, Duesterwald et al. [12] used genome sequence data and a machine-learning approach to predict cycle threshold (Ct) values of SARS-CoV-2 infections based on the *k*-mers. Similar to our findings, they suggested that S:L452 and P681 were hallmarks of VOCs, implying impacts on the observed Ct values in clinical samples. Although the machine-learning approach may capture broader patterns and interactions within the genome on Ct values, they lack interpretability compared to regression models. For example, regression-based models could offer insights into the direct association between specific genetic variants and viral copies. In addition, regression-based models may perform well even with limited sample sizes [19], provided that the assumptions of the model are met and the predictors are informative, whereas using machine-learning methods with small sample sizes can be challenging.

With the availability of high-quality whole-genome sequences for SARS-CoV-2, we demonstrated that GWAS analysis of the viral genome can identify SNPs that associate with positive or negative impacts on viral copies in VOCs, revealing important biological insights and enhancing our understanding of within-host viral dynamics. We argue that the application of GWAS analyses to study viral genomes provides a particularly tractable tool to identify potential SNPs of interest for further evaluation using genetic engineering for several reasons. First, the small genome size of viruses and high evolutionary rates make it easier to perform comprehensive genome-wide scans for SNPs and to experimentally test the impacts of SNPs on specific traits. Second, significant phenotypic variations (e.g., viral loads and antibody responses) are often observed in viral infections, despite limited changes in the viral genome. GWAS can help to identify SNPs that correlate with these phenotypic variations, providing insights into the genetic basis of these traits. Third, the increasing accessibility to sequence viral genomes makes it possible to perform GWAS on rich datasets, enabling in-depth analysis of the temporal dynamics of viral evolution. Together, the applicability of GWAS analyses to study viral genomes can provide a new approach for exploring the intricate interplay between genetic mutations and phenotypes, informing strategies for managing and mitigating the impact of emerging viral variants, and contributing to the development of potential therapeutic interventions.

Materials & Methods

Ethics

The Institutional Review Board from the Yale University Human Research Protection Program determined that the RT-qPCR testing and sequencing of de-identified remnant COVID-19 clinical samples obtained from clinical partners conducted in this study is not research involving human subjects (IRB Protocol ID: 2000028599).

Clinical sample collection and measurement of viral copies by RT-qPCR

SARS-CoV-2 positive samples (nasal swabs in viral transport media) were collected through the Yale New Haven Hospital (YNHH) System as a part of routine inpatient and outpatient testing and sent to the Yale SARS-CoV-2 Genomic Surveillance Initiative. Using the MagMAX viral/pathogen nucleic acid isolation kit, nucleic acid was extracted from 300µl of each clinical sample and eluted into 75µl of elution buffer. Extracted nucleic acid was then used as template for a "research use only" (RUO) RT-qPCR assay [21] to test for presence of SARS-CoV-2 RNA. Ct values from the nucleocapsid target (CDC-N1 primer-probe set [52]) were used to derive viral copy numbers using a previously determined standard curve for this primer set [53]. A positive RNA control with defined viral copy number (1000/µl) was used to standardize results across individual runs.

Whole genome sequencing

Libraries were prepared for sequencing using the Illumina COVIDSeq Test (RUO version) and quantified using the Qubit High Sensitivity dsDNA kit. Negative controls were included for RNA extraction, cDNA synthesis, and amplicon generation. Prepared libraries were sequenced at the Yale Center for Genomic Analysis on the Illumina NovaSeq with a 2x150 approach and at least 1 million reads per sample.

Reads were then aligned to the Wuhan-Hu-1 reference genome (GenBank MN908937.3) using BWA-MEM v.0.7.15 [54]. Adaptor sequences were then trimmed, primer sequences masked, and consensus genomes called (simple majority >60% frequency) using iVar v1.3.133 [55] and SAMtools v1.11 [56]. When <20 reads were present at a site an ambiguous "N" was used, with negative controls consisting of ≥99% Ns. The Pangolin lineage assignment tool [57] was used for assigning viral lineages.

Clinical metadata

We obtained patient metadata and vaccination records from the YNHH system and the Center for Outcomes Research and Evaluation (CORE) and matched these records to sequencing data through unique sample identifiers. Duplicate patient records or those with missing or inconsistent metadata and vaccination date were removed from the GWAS analysis. We also removed patient records with persistent infections.

We determined vaccination status at time of infection by comparing the sample collection date to the patient's vaccination record dates. We categorized vaccine statuses based on the number of vaccine doses received at least 14 days before the collection date. Patient

vaccination statuses at the time of infection were categorized as follows: non-vaccine, one-dose vaccine, two-dose vaccine, two-dose vaccine with one booster, or two-dose vaccine with two boosters. We calculated the age of each patient as the difference between the date of birth and the sampling date.

Single nucleotide polymorphisms

To identify single nucleotide polymorphisms (SNPs), we first aligned the 9902 genome sequences using *nextalign* (v3.2.1) [58] with the reference genome of the Wuhan-Hu-1 genome (GenBank accession: MN908937.3). Then, SNPs were identified using *snp-sites* (v2.4.1) [59], with the reference genome of the Wuhan-Hu-1 genome (GenBank accession: MN908937.3). We also normalized the SNPs in the generated VCF file, such that multiallelic SNPs were separated into different rows. Normalizing the SNPs ensured that each SNP was one-hot encoded and analyzed separately. Note that we did not include ambiguous SNPs, deletions and insertions in our GWAS analysis. We used *vcf-annotator* (v0.7) to annotate SNPs to corresponding amino acid changes.

Multidimensional scaling and population control

To reveal the underlying structure of the 9902 genome sequences. We first used *snp-dists* (v0.7.0) [60] to convert the aligned sequences (a FASTA alignment) to a SNP distance matrix. We then applied a multidimensional scaling (MDS) method [24] to transform the SNP distance matrix into a geometric configuration while preserving the original pairwise relationships. The scaling was conducted using *cmdscale* function in an R package *stats* (v3.6.2). We set the maximal dimensional parameter $k = 2$.

To measure the goodness of the transformation, we calculated the distance between the original genome sequencing data and compared it with the new distances determined by MDS. This involved arranging the two matrices of distances into two columns and computing the correlation coefficient (i.e., r) between them. Finally, we used r^2 to measure the proportion of variance in the original distance matrix explained by the new computed distance matrix.

Testing for associations between viral copies and SNPs

In this work, we conducted a series of single SNP regression analyses to test for associations between viral copies and SNPs. The linear regression model is written as follows:

$$Y \sim \alpha W + \beta_i SNP_i + \xi_1 d_1 + \xi_2 d_2 + e,$$

where Y is a vector of normalized $\log_{10}$-transformed viral copies, W is a matrix of covariates, including age (a categorical variable with four age groups of “<18”, “18-49”, “50-69”, and “>70” years old), vaccination status (a categorical variable with vaccination statuses of “0 doses”, “1 dose”, “2 doses”, “2 doses and 1 booster”, “2 doses and 2 boosters”) and an intercept, and α is a vector that corresponds to coefficients of the covariates. In particular, SNP_i is a vector of genotype values for all samples at each SNP, i. It is a binary variable: 0 represents the SNP is not present in the genome sequence, whereas 1 represents its presence. β_i is the effective size of each identified SNP, i. The vectors d_1, d_2 represent the two dimensions computed by MDS, and ξ_1, ξ_2 are the coefficients of the dimension covariates. The random effect of residual errors is presented by e, which is assumed to follow a normal distribution with a mean of 0 and a standard deviation of σ_e.

Phylogenetic tree construction and comparison to variant-defining substitutions

We employed *iq-tree* (v2.2.2.6) [61] of a representative set using 996 of our 9902 genome sequences for tree construction, using Wuhan-Hu-1 (GenBank MN908937.3) as the reference genome. The variant-defining amino acid changes were defined as those mutations with >75% prevalence in at least one lineage, as estimated on outbreak.info website [33]. Note that we did not include deletions in variant-defining substitutions.

Data and code availability

We used the R statistical software (v4.0.2) for all statistical analyses and visualization. Data and code used in this study are publicly available on Github: https://github.com/grubaughlab/2024_paper_GWAS. All genome sequences used for the GWAS analysis and a subset of the associated metadata (accession number, virus name, collection date, originating lab and submitting lab, and the list of authors) in this dataset are published in GISAID's EpiCoV database: https://doi.org/10.55876/gis8.240219fh. The de-identified and coded clinical metadata associated with the sequenced samples are available upon request with IRB approval.

Acknowledgements

We would like to thank Verity Hill, Seth Redmond, Jiye Kwon, Rafael Lopes, Sophie Taylor, and Philip Jack for their helpful conversations and feedback on this work. This project is supported by the Centers for Disease Control and Prevention (CDC) Broad Agency Announcement Contract 75D30122C14697 (NDG). This work does not necessarily represent the views of the CDC.

Competing Interest Statement

NDG is a paid consultant for BioNTech, DMW has received consulting fees from Pfizer, Merck, and GSK, unrelated to this manuscript, and has been PI on research grants from Pfizer and Merck to Yale, unrelated to this manuscript.

Yale SARS-CoV-2 Genomic Surveillance Initiative Authors

Tara Alpert, Kaya Bilguvar, Kendall Billig, Mallery Breban, Anderson Brito, Christopher Castaldi, Rebecca Earnest, Bony De Kumar, Joseph Fauver, Chaney Kalinich, Tobias Koch, Marie Landry, Shrikant Mane, Isabel Ott, David Peaper, Mary Petrone, Kien Pham, Jessica Rothman, Irina Tikhonova, Chantal Vogels, Anne Watkins

References

1. Killingley B, Mann AJ, Kalinova M, Boyers A, Goonawardane N, Zhou J, et al. Safety, tolerability and viral kinetics during SARS-CoV-2 human challenge in young adults. Nat Med. 2022;28: 1031–1041. doi:10.1038/s41591-022-01780-9

2. Marks M, Millat-Martinez P, Ouchi D, Roberts CH, Alemany A, Corbacho-Monné M, et al. Transmission of COVID-19 in 282 clusters in Catalonia, Spain: a cohort study. Lancet Infect Dis. 2021;21: 629–636. doi:10.1016/S1473-3099(20)30985-3

3. Jones TC, Biele G, Mühlemann B, Veith T, Schneider J, Beheim-Schwarzbach J, et al. Estimating infectiousness throughout SARS-CoV-2 infection course. Science. 2021;373. doi:10.1126/science.abi5273

4. Cevik M, Tate M, Lloyd O, Maraolo AE, Schafers J, Ho A. SARS-CoV-2, SARS-CoV, and MERS-CoV viral load dynamics, duration of viral shedding, and infectiousness: a systematic review and meta-analysis. Lancet Microbe. 2021;2: e13–e22. doi:10.1016/S2666-5247(20)30172-5

5. Singanayagam A, Patel M, Charlett A, Lopez Bernal J, Saliba V, Ellis J, et al. Duration of infectiousness and correlation with RT-PCR cycle threshold values in cases of COVID-19, England, January to May 2020. Euro Surveill. 2020;25. doi:10.2807/1560-7917.ES.2020.25.32.2001483

6. Singanayagam A, Hakki S, Dunning J, Madon KJ, Crone MA, Koycheva A, et al. Community transmission and viral load kinetics of the SARS-CoV-2 delta (B.1.617.2) variant in vaccinated and unvaccinated individuals in the UK: a prospective, longitudinal, cohort study. Lancet Infect Dis. 2022;22: 183–195. doi:10.1016/S1473-3099(21)00648-4

7. Kissler SM, Fauver JR, Mack C, Tai CG, Breban MI, Watkins AE, et al. Viral Dynamics of SARS-CoV-2 Variants in Vaccinated and Unvaccinated Persons. N Engl J Med. 2021;385: 2489–2491. doi:10.1056/NEJMc2102507

8. Puhach O, Adea K, Hulo N, Sattonnet P, Genecand C, Iten A, et al. Infectious viral load in unvaccinated and vaccinated individuals infected with ancestral, Delta or Omicron SARS-CoV-2. Nat Med. 2022;28: 1491–1500. doi:10.1038/s41591-022-01816-0

9. Boucau J, Marino C, Regan J, Uddin R, Choudhary MC, Flynn JP, et al. Duration of Shedding of Culturable Virus in SARS-CoV-2 Omicron (BA.1) Infection. N Engl J Med. 2022;387: 275–277. doi:10.1056/NEJMc2202092

10. Hay JA, Kennedy-Shaffer L, Kanjilal S, Lennon NJ, Gabriel SB, Lipsitch M, et al. Estimating epidemiologic dynamics from cross-sectional viral load distributions. Science. 2021;373. doi:10.1126/science.abh0635

11. Fryer HR, Golubchik T, Hall M, Fraser C, Hinch R, Ferretti L, et al. Viral burden is associated with age, vaccination, and viral variant in a population-representative study of SARS-CoV-2 that accounts for time-since-infection-related sampling bias. PLoS Pathog. 2023;19: e1011461. doi:10.1371/journal.ppat.1011461

12. Duesterwald L, Nguyen M, Christensen P, Wesley Long S, Olsen RJ, Musser JM, et al. Using Genome Sequence Data to Predict SARS-CoV-2 Detection Cycle Threshold Values. doi:10.1101/2022.11.14.22282297

13. Uffelmann E, Huang QQ, Munung NS, de Vries J, Okada Y, Martin AR, et al. Genome-wide association studies. Nature Reviews Methods Primers. 2021;1: 1–21. doi:10.1038/s43586-021-00056-9

14. McLaren PJ, Porreca I, Iaconis G, Mok HP, Mukhopadhyay S, Karakoc E, et al. Africa-specific

656 human genetic variation near CHD1L associates with HIV-1 load. Nature. 2023;620: 1025–1030.
657 doi:10.1038/s41586-023-06370-4

658 15. Karim M, Dunham I, Ghoussaini M. Mining a GWAS of Severe Covid-19. The New England
659 journal of medicine. 2020. pp. 2588–2589. doi:10.1056/NEJMc2025747

660 16. Roberts GHL, Partha R, Rhead B, Knight SC, Park DS, Coignet MV, et al. Expanded COVID-19
661 phenotype definitions reveal distinct patterns of genetic association and protective effects. Nat
662 Genet. 2022;54: 374–381. doi:10.1038/s41588-022-01042-x

663 17. Genomewide Association Study of Severe Covid-19 with Respiratory Failure. N Engl J Med.
664 2020;383: 1522–1534. doi:10.1056/NEJMoa2020283

665 18. Power RA, Parkhill J, de Oliveira T. Microbial genome-wide association studies: lessons from
666 human GWAS. Nat Rev Genet. 2017;18: 41–50. doi:10.1038/nrg.2016.132

667 19. Power RA, Davaniah S, Derache A, Wilkinson E, Tanser F, Gupta RK, et al. Genome-Wide
668 Association Study of HIV Whole Genome Sequences Validated using Drug Resistance. PLoS
669 One. 2016;11: e0163746. doi:10.1371/journal.pone.0163746

670 20. Ansari MA, Pedergnana V, L C Ip C, Magri A, Von Delft A, Bonsall D, et al. Genome-to-genome
671 analysis highlights the effect of the human innate and adaptive immune systems on the hepatitis
672 C virus. Nat Genet. 2017;49: 666–673. doi:10.1038/ng.3835

673 21. Vogels CBF, Breban MI, Ott IM, Alpert T, Petrone ME, Watkins AE, et al. Multiplex qPCR
674 discriminates variants of concern to enhance global surveillance of SARS-CoV-2. PLoS Biol.
675 2021;19: e3001236. doi:10.1371/journal.pbio.3001236

676 22. Zhou C, Zhang T, Ren H, Sun S, Yu X, Sheng J, et al. Impact of age on duration of viral RNA
677 shedding in patients with COVID-19. Aging . 2020;12: 22399–22404. doi:10.18632/aging.104114

678 23. Acharya CB, Schrom J, Mitchell AM, Coil DA, Marquez C, Rojas S, et al. Viral Load Among
679 Vaccinated and Unvaccinated, Asymptomatic and Symptomatic Persons Infected With the
680 SARS-CoV-2 Delta Variant. Open Forum Infect Dis. 2022;9: ofac135. doi:10.1093/ofid/ofac135

681 24. Torgerson WS. Multidimensional scaling: I. Theory and method. Psychometrika. 1952;17: 401–
682 419. doi:10.1007/bf02288916

683 25. VanderWeele TJ, Mathur MB. SOME DESIRABLE PROPERTIES OF THE BONFERRONI
684 CORRECTION: IS THE BONFERRONI CORRECTION REALLY SO BAD? Am J Epidemiol.
685 2018;188: 617–618. doi:10.1093/aje/kwy250

686 26. Ward IL, Bermingham C, Ayoubkhani D, Gethings OJ, Pouwels KB, Yates T, et al. Risk of covid-
687 19 related deaths for SARS-CoV-2 omicron (B.1.1.529) compared with delta (B.1.617.2):
688 retrospective cohort study. BMJ. 2022;378: e070695. doi:10.1136/bmj-2022-070695

689 27. Volz E, Hill V, McCrone JT, Price A, Jorgensen D, O'Toole Á, et al. Evaluating the Effects of
690 SARS-CoV-2 Spike Mutation D614G on Transmissibility and Pathogenicity. Cell. 2021;184: 64–
691 75.e11. doi:10.1016/j.cell.2020.11.020

692 28. Tian D, Sun Y, Zhou J, Ye Q. The Global Epidemic of the SARS-CoV-2 Delta Variant, Key Spike
693 Mutations and Immune Escape. Front Immunol. 2021;12: 751778.
694 doi:10.3389/fimmu.2021.751778

695 29. Hodcroft EB, Domman DB, Snyder DJ, Oguntuyo KY, Van Diest M, Densmore KH, et al.
696 Emergence in late 2020 of multiple lineages of SARS-CoV-2 Spike protein variants affecting
697 amino acid position 677. medRxiv. 2021. doi:10.1101/2021.02.12.21251658

698 30. Cosar B, Karagulleoglu ZY, Unal S, Ince AT, Uncuoglu DB, Tuncer G, et al. SARS-CoV-2
699 Mutations and their Viral Variants. Cytokine Growth Factor Rev. 2022;63: 10–22.
700 doi:10.1016/j.cytogfr.2021.06.001

31. Chen J, Wang R, Wang M, Wei G-W. Mutations Strengthened SARS-CoV-2 Infectivity. J Mol Biol. 2020;432: 5212–5226. doi:10.1016/j.jmb.2020.07.009

32. Harvey WT, Carabelli AM, Jackson B, Gupta RK, Thomson EC, Harrison EM, et al. SARS-CoV-2 variants, spike mutations and immune escape. Nat Rev Microbiol. 2021;19: 409–424. doi:10.1038/s41579-021-00573-0

33. Gangavarapu K, Latif AA, Mullen JL, Alkuzweny M, Hufbauer E, Tsueng G, et al. Outbreak.info genomic reports: scalable and dynamic surveillance of SARS-CoV-2 variants and mutations. Nat Methods. 2023;20: 512–522. doi:10.1038/s41592-023-01769-3

34. Tang X, Wu C, Li X, Song Y, Yao X, Wu X, et al. On the origin and continuing evolution of SARS-CoV-2. Natl Sci Rev. 2020;7: 1012–1023. doi:10.1093/nsr/nwaa036

35. Carabelli AM, Peacock TP, Thorne LG, Harvey WT, Hughes J, COVID-19 Genomics UK Consortium, et al. SARS-CoV-2 variant biology: immune escape, transmission and fitness. Nat Rev Microbiol. 2023;21: 162–177. doi:10.1038/s41579-022-00841-7

36. Souza PFN, Mesquita FP, Amaral JL, Landim PGC, Lima KRP, Costa MB, et al. The spike glycoprotein of SARS-CoV-2: A review of how mutations of spike glycoproteins have driven the emergence of variants with high transmissibility and immune escape. Int J Biol Macromol. 2022;208: 105–125. doi:10.1016/j.ijbiomac.2022.03.058

37. Kimura I, Kosugi Y, Wu J, Zahradnik J, Yamasoba D, Butlertanaka EP, et al. The SARS-CoV-2 Lambda variant exhibits enhanced infectivity and immune resistance. Cell Rep. 2022;38: 110218. doi:10.1016/j.celrep.2021.110218

38. Yadav PD, Bergeron É, Flora MS. Emerging SARS-COV-2 Variants: Genomic Variations, Transmission, Pathogenesis, Clinical Impact and Interventions. Frontiers Media SA; 2023. Available: https://play.google.com/store/books/details?id=AHi6EAAAQBAJ

39. BMvd V, Dingemans J, Bank LE, von Wintersdorff CJ. Viral load dynamics in healthcare workers with COVID-19 during Delta and Omicron era. [cited 10 Feb 2024]. Available: https://europepmc.org/article/ppr/ppr485029

40. Lentini A, Pereira A, Winqvist O, Reinius B. Monitoring of the SARS-CoV-2 Omicron BA.1/BA.2 variant transition in the Swedish population reveals higher viral quantity in BA.2 cases. bioRxiv. 2022. doi:10.1101/2022.03.26.22272984

41. Russell TW, Townsley H, Abbott S, Hellewell J, Carr EJ, Chapman LAC, et al. Combined analyses of within-host SARS-CoV-2 viral kinetics and information on past exposures to the virus in a human cohort identifies intrinsic differences of Omicron and Delta variants. PLoS Biol. 2024;22: e3002463. doi:10.1371/journal.pbio.3002463

42. Kopsidas I, Karagiannidou S, Kostaki EG, Kousi D, Douka E, Sfikakis PP, et al. Global Distribution, Dispersal Patterns, and Trend of Several Omicron Subvariants of SARS-CoV-2 across the Globe. Trop Med Infect Dis. 2022;7. doi:10.3390/tropicalmed7110373

43. Motozono C, Toyoda M, Tan TS, Hamana H, Goto Y, Aritsu Y, et al. The SARS-CoV-2 Omicron BA.1 spike G446S mutation potentiates antiviral T-cell recognition. Nat Commun. 2022;13: 5440. doi:10.1038/s41467-022-33068-4

44. Lin X, Sha Z, Trimpert J, Kunec D, Jiang C, Xiong Y, et al. The NSP4 T492I mutation increases SARS-CoV-2 infectivity by altering non-structural protein cleavage. Cell Host Microbe. 2023;31: 1170–1184.e7. doi:10.1016/j.chom.2023.06.002

45. Luo CH, Morris CP, Sachithanandham J, Amadi A, Gaston D, Li M, et al. Infection with the SARS-CoV-2 Delta Variant is Associated with Higher Infectious Virus Loads Compared to the Alpha Variant in both Unvaccinated and Vaccinated Individuals. medRxiv. 2021. doi:10.1101/2021.08.15.21262077

46. von Wintersdorff CJH, Dingemans J, van Alphen LB, Wolffs PFG, van der Veer BMJW, Hoebe CJPA, et al. Infections with the SARS-CoV-2 Delta variant exhibit fourfold increased viral loads in the upper airways compared to Alpha or non-variants of concern. Sci Rep. 2022;12: 13922. doi:10.1038/s41598-022-18279-5

47. Li B, Deng A, Li K, Hu Y, Li Z, Shi Y, et al. Viral infection and transmission in a large, well-traced outbreak caused by the SARS-CoV-2 Delta variant. Nat Commun. 2022;13: 460. doi:10.1038/s41467-022-28089-y

48. Fall A, Eldesouki RE, Sachithanandham J, Morris CP, Norton JM, Gaston DC, et al. The displacement of the SARS-CoV-2 variant Delta with Omicron: An investigation of hospital admissions and upper respiratory viral loads. EBioMedicine. 2022;79: 104008. doi:10.1016/j.ebiom.2022.104008

49. Hay JA, Kissler SM, Fauver JR, Mack C, Tai CG, Samant RM, et al. Quantifying the impact of immune history and variant on SARS-CoV-2 viral kinetics and infection rebound: A retrospective cohort study. Elife. 2022;11. doi:10.7554/eLife.81849

50. Jones RP, Ponomarenko A. COVID-19-Related Age Profiles for SARS-CoV-2 Variants in England and Wales and States of the USA (2020 to 2022): Impact on All-Cause Mortality. Infect Dis Rep. 2023;15: 600–634. doi:10.3390/idr15050058

51. Bartha I, Carlson JM, Brumme CJ, McLaren PJ, Brumme ZL, John M, et al. A genome-to-genome analysis of associations between human genetic variation, HIV-1 sequence diversity, and viral control. Elife. 2013;2: e01123. doi:10.7554/eLife.01123

52. Lu X, Wang L, Sakthivel SK, Whitaker B, Murray J, Kamili S, et al. US CDC Real-Time Reverse Transcription PCR Panel for Detection of Severe Acute Respiratory Syndrome Coronavirus 2. Emerg Infect Dis. 2020;26: 1654–1665. doi:10.3201/eid2608.201246

53. Vogels CBF, Brito AF, Wyllie AL, Fauver JR, Ott IM, Kalinich CC, et al. Analytical sensitivity and efficiency comparisons of SARS-CoV-2 RT–qPCR primer–probe sets. Nature Microbiology. 2020;5: 1299–1305. doi:10.1038/s41564-020-0761-6

54. Li H. Aligning sequence reads, clone sequences and assembly contigs with BWA-MEM. arXiv [q-bio.GN]. 2013. Available: http://arxiv.org/abs/1303.3997

55. Grubaugh ND, Gangavarapu K, Quick J, Matteson NL, De Jesus JG, Main BJ, et al. An amplicon-based sequencing framework for accurately measuring intrahost virus diversity using PrimalSeq and iVar. Genome Biol. 2019;20: 8. doi:10.1186/s13059-018-1618-7

56. Danecek P, Bonfield JK, Liddle J, Marshall J, Ohan V, Pollard MO, et al. Twelve years of SAMtools and BCFtools. Gigascience. 2021;10. doi:10.1093/gigascience/giab008

57. O'Toole Á, Scher E, Underwood A, Jackson B, Hill V, McCrone JT, et al. Assignment of epidemiological lineages in an emerging pandemic using the pangolin tool. Virus Evol. 2021;7: veab064. doi:10.1093/ve/veab064

58. Aksamentov I, Roemer C, Hodcroft E, Neher R. Nextclade: clade assignment, mutation calling and quality control for viral genomes. J Open Source Softw. 2021;6: 3773. doi:10.21105/joss.03773

59. Page AJ, Taylor B, Delaney AJ, Soares J, Seemann T, Keane JA, et al. SNP-sites: rapid efficient extraction of SNPs from multi-FASTA alignments. Microb Genom. 2016;2: e000056. doi:10.1099/mgen.0.000056

60. Creators Seemann, Torsten1 Show affiliations 1. The University of Melbourne. Source code for snp-dists software. doi:10.5281/zenodo.1411986

61. Minh BQ, Schmidt HA, Chernomor O, Schrempf D, Woodhams MD, von Haeseler A, et al.

Corrigendum to: IQ-TREE 2: New Models and Efficient Methods for Phylogenetic Inference in the Genomic Era. Mol Biol Evol. 2020;37: 2461. doi:10.1093/molbev/msaa131

Supplementary Figures & Tables

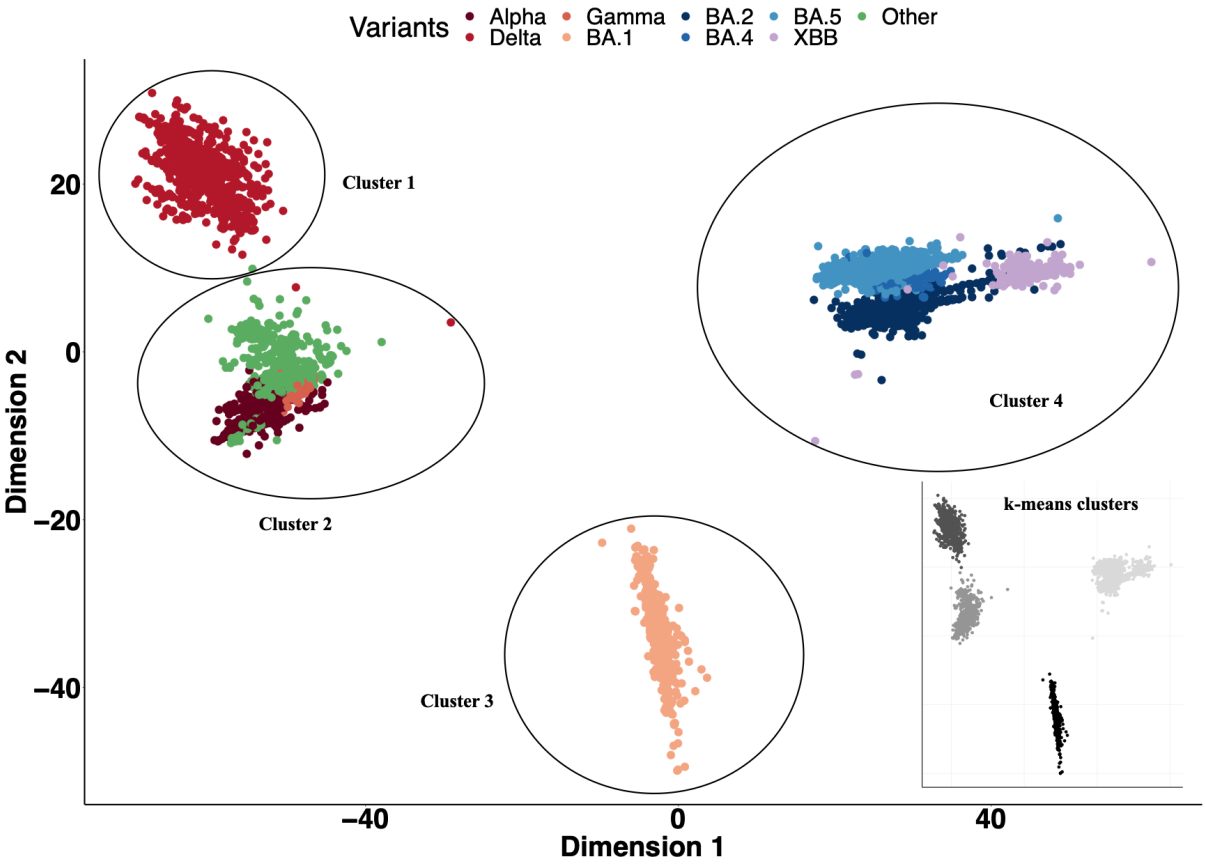

Supplements Figure 1. Results of multidimensional scaling. The population structure of the 9902 genome sequences using a multidimensional scaling (MDS) method. Clusters are defined using a *k*-means clustering method, as shown on the bottom right corner.

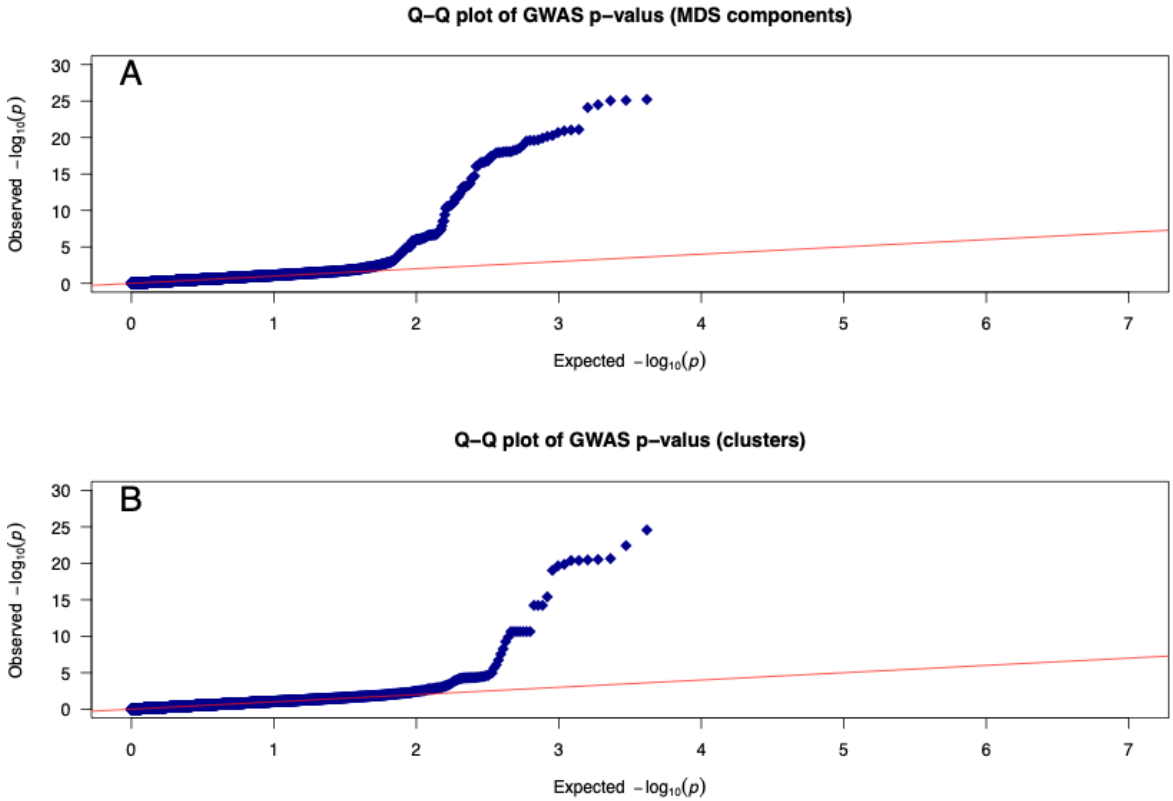

Supplements Figure 2. Q-Q plots of GWAS p-values. Q-Q plots (quantile-quantile plots) showing the p-values from GWAS analysis using **(A)** two MDS-computed components, or **(B)** MDS-inferred four clusters as covariates in the regression model.

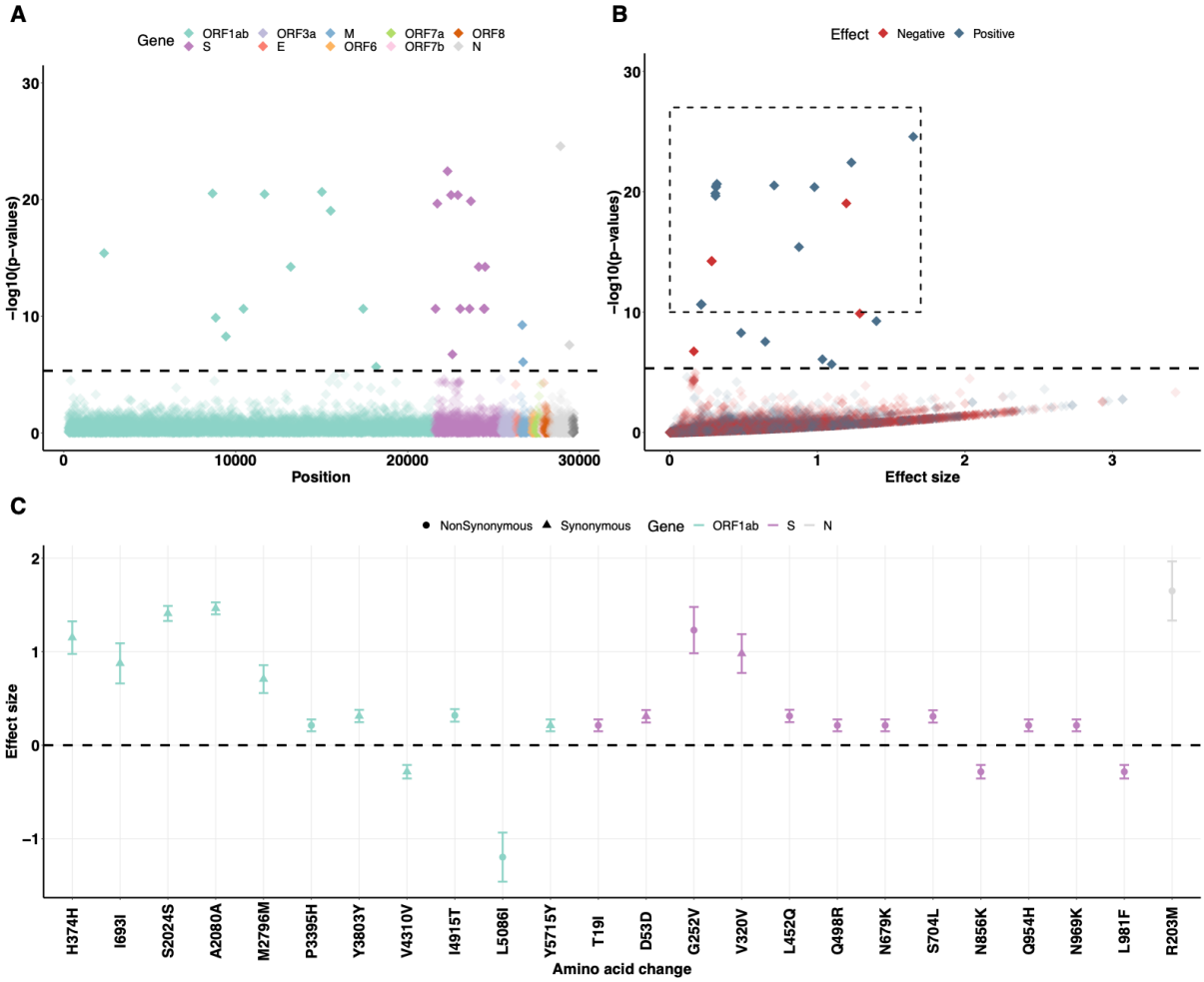

Supplemental Figure 3. GWAS analysis using the four clusters (shown in Fig. S1) as covariates for population control. (**A**) Genome-wide association results of the impact of identified SNPs on viral copies during SARS-CoV-2 infection. The dashed line indicates the permuted threshold for genome-wide significance $p = 4.67 \times 10^{-6}$ (0.05/10697 SNPs). Significant SNPs are shown with solid colors. (**B**) SNPs (with $p < 1 \times 10^{-10}$) that have positive (blue) or negative (red) effects on viral copies. (**C**) The corresponding synonymous (triangles) and non-synonymous (circles) amino acid changes that associate with increased or decreased viral copies. Data shown as means with 95% confidence intervals. The estimated effective sizes and associated standard deviations are given **Table S2**.

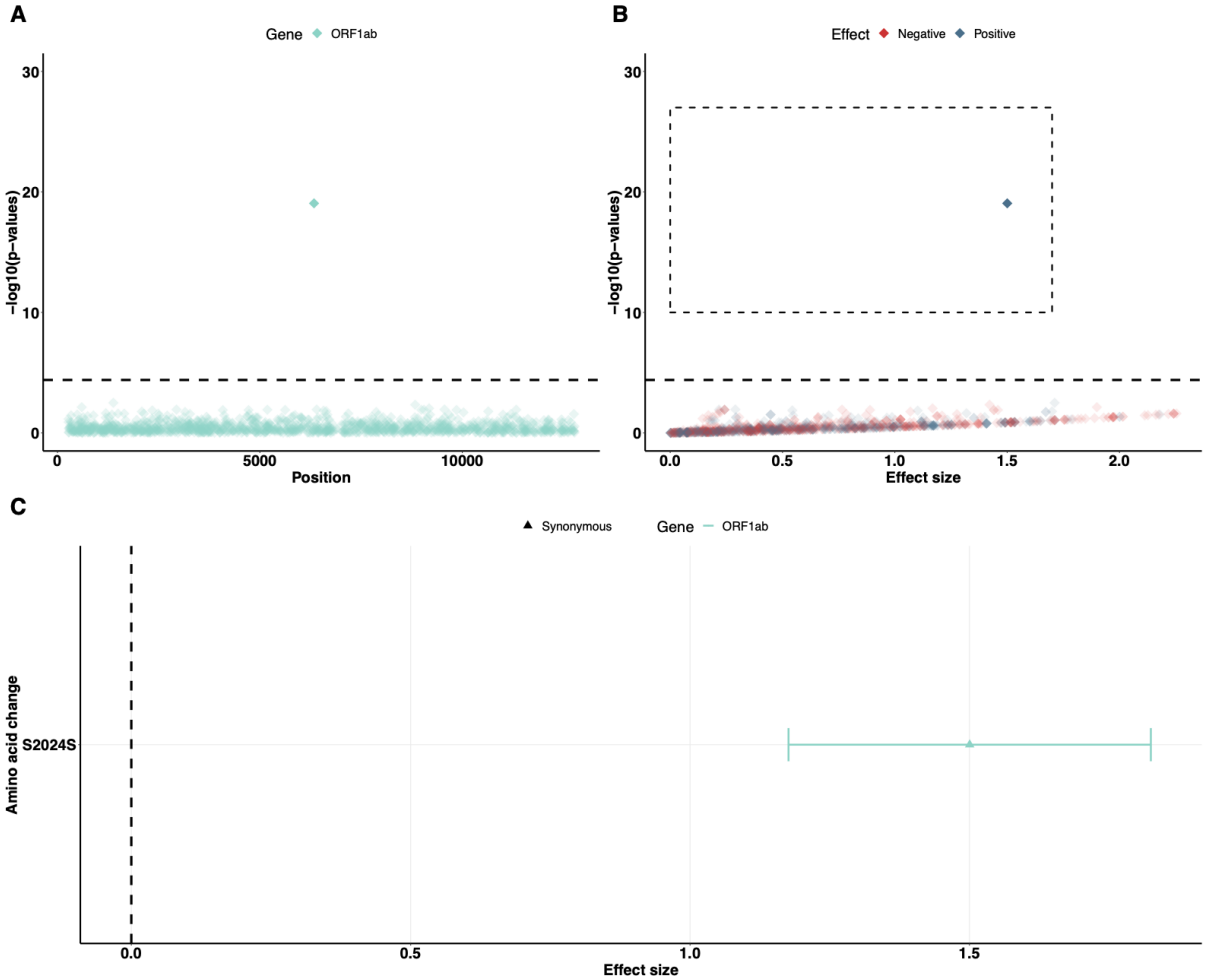

Supplemental Figure 4. GWAS analysis using only Cluster 1 data (shown in Fig. S1). (**A**) Genome-wide association results of the impact of identified SNPs on viral copies during SARS-CoV-2 infection. The dashed line indicates the permuted threshold for genome-wide significance $p = 4.03 \times 10^{-5}$ (0.05/1242 SNPs). Significant SNPs are shown with solid colors. (**B**) SNPs (with $p < 1 \times 10^{-10}$) that have positive (blue) or negative (red) effects on viral copies. (**C**) The corresponding synonymous (triangles) amino acid changes that associate with increased or decreased viral copies. Data shown as means with 95% confidence intervals.

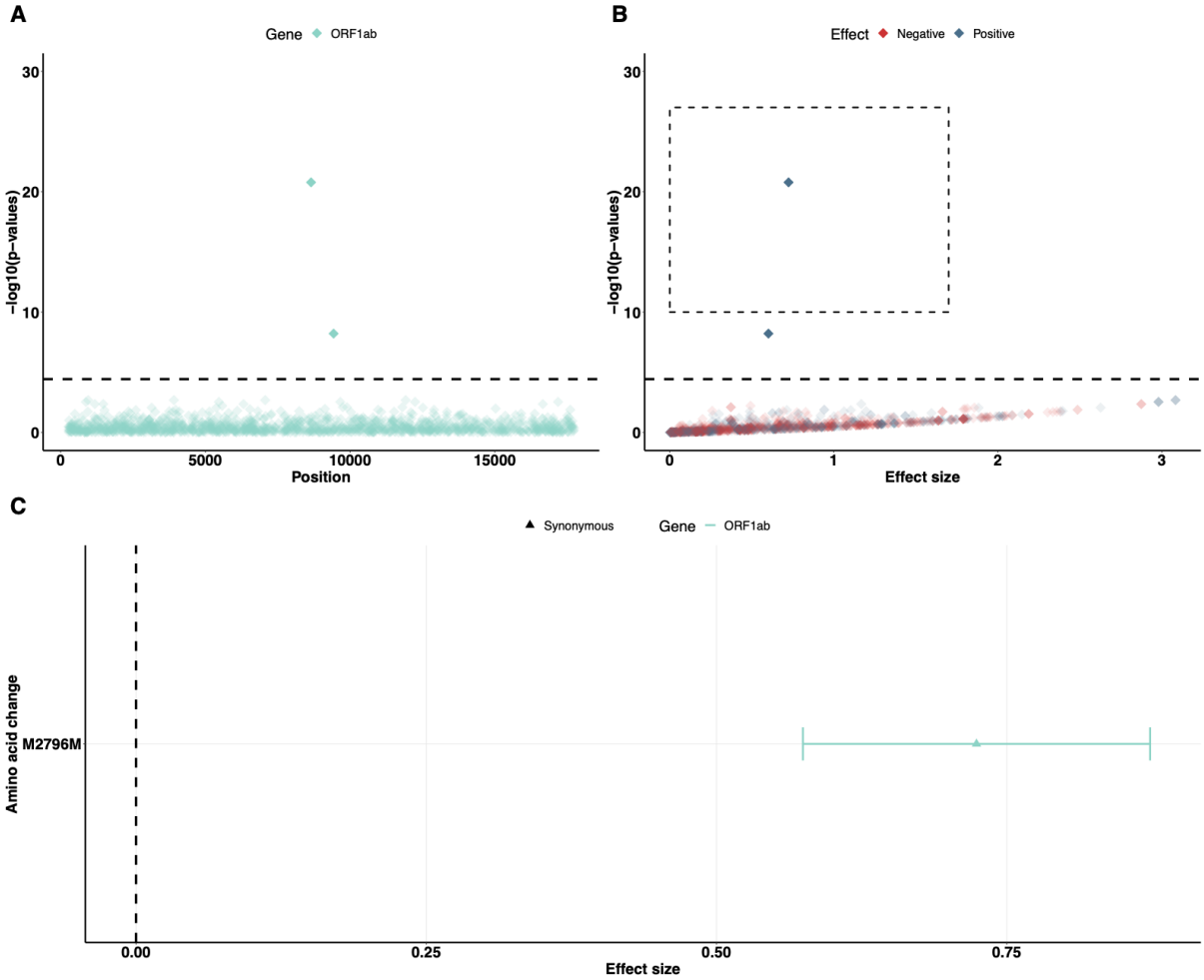

Supplemental Figure 5. GWAS analysis using Cluster 2 data (shown in Fig. S1). (**A**) Genome-wide association results of the impact of identified SNPs on viral copies during SARS-CoV-2 infection. The dashed line indicates the permuted threshold for genome-wide significance $p = 3.68 \times 10^{-5}$ (0.05/1357 SNPs). Significant SNPs are shown with solid colors. (**B**) SNPs (with $p < 1 \times 10^{-10}$) that have positive (blue) or negative (red) effects on viral copies. (**C**) The corresponding synonymous (triangles) amino acid changes that associate with increased or decreased viral copies. Data shown as means with 95% confidence intervals.

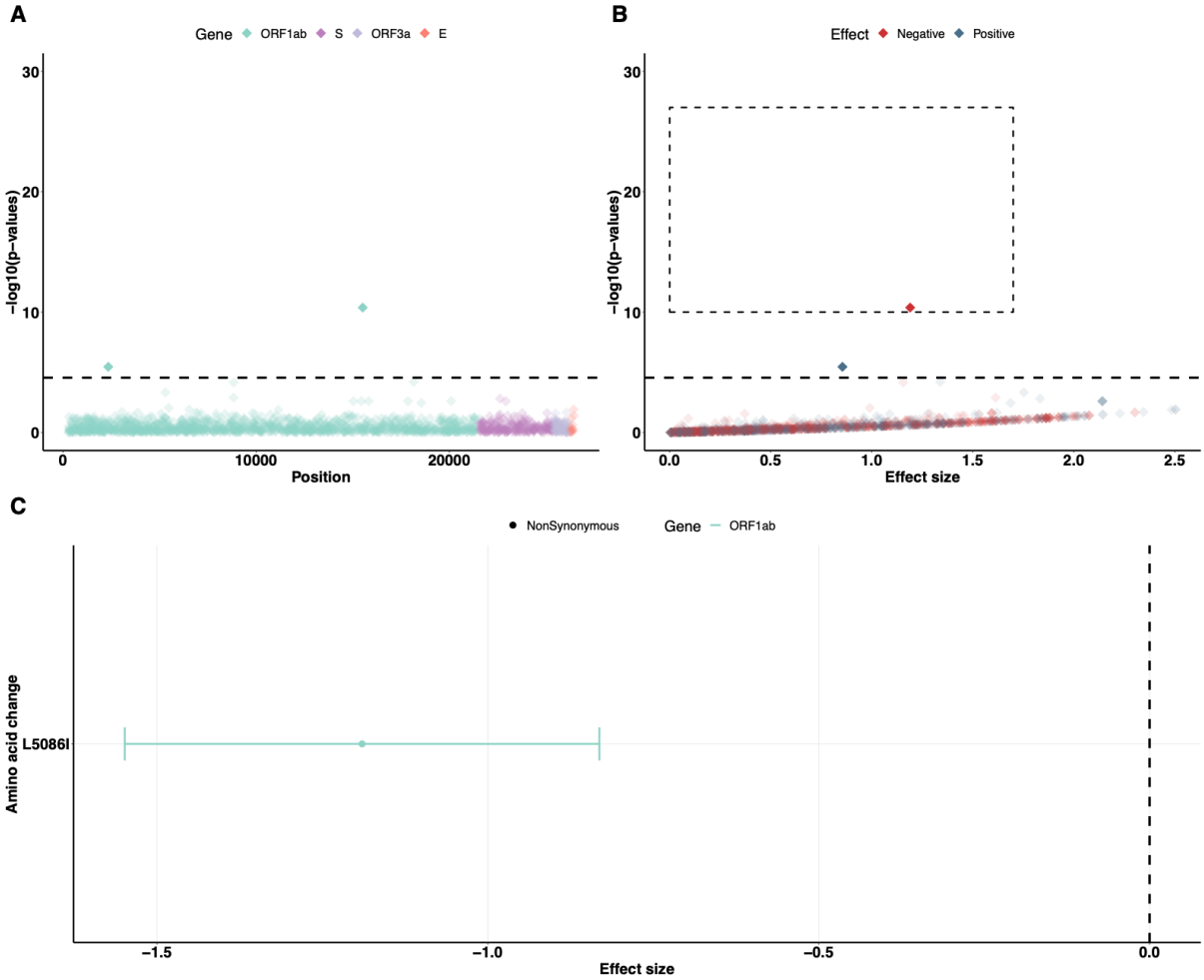

Supplemental Figure 6. GWAS analysis using Cluster 3 data (shown in Fig. S1). (**A**) Genome-wide association results of the impact of identified SNPs on viral copies during SARS-CoV-2 infection. The dashed line indicates the permuted threshold for genome-wide significance $p = 2.80 \times 10^{-5}$ (0.05/1784 SNPs). Significant SNPs are shown with solid colors. (**B**) SNPs (with $p < 1 \times 10^{-10}$) that have positive (blue) or negative (red) effects on viral copies. (**C**) The corresponding non-synonymous (circles) amino acid changes that associate with increased or decreased viral copies. Data shown as means with 95% confidence intervals.

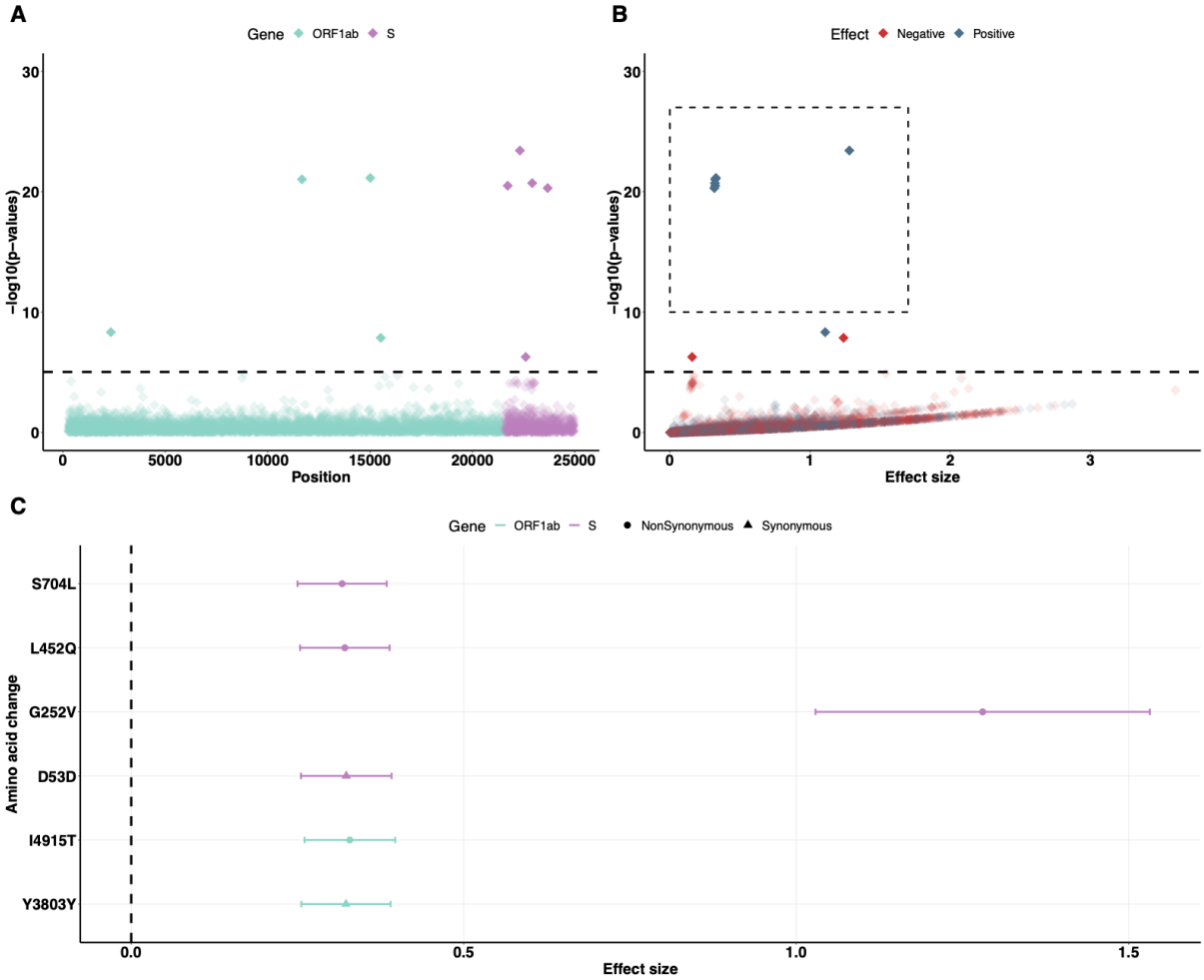

Supplemental Figure 7. GWAS analysis using Cluster 4 data (shown in Fig. S1). (**A**) Genome-wide association results of the impact of identified SNPs on viral copies during SARS-CoV-2 infection. The dashed line indicates the permuted threshold for genome-wide significance $p = 7.91 \times 10^{-6}$ (0.05/6314 SNPs). Significant SNPs are shown with solid colors. (**B**) SNPs (with $p < 1 \times 10^{-10}$) that have positive (blue) or negative (red) effects on viral copies. (**C**) The corresponding synonymous (triangles) and non-synonymous (circles) amino acid changes that associate with increased or decreased viral copies. Data shown as means with 95% confidence intervals.

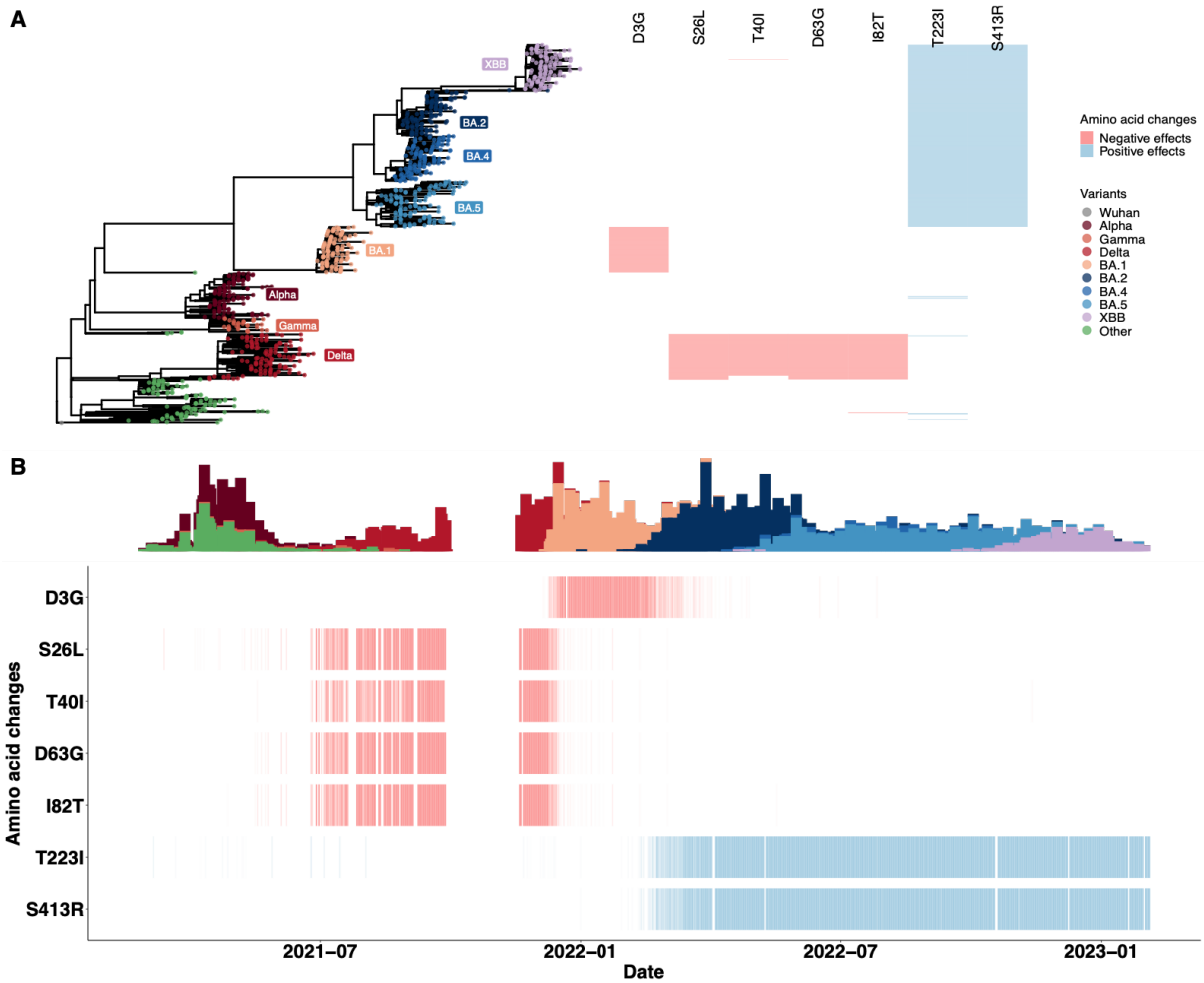

Supplemental Figure 8. The temporal dynamics of amino acid changes in the ORF3a gene (S26L and T223I), M gene (D3G and I82T), ORF7b gene (T40I) and N gene (D63G and S413R) associated with changes in viral copies. The results are based on the multivariate regression analysis using the two MDS components as covariates. (**A**) The phylogenetic tree estimated from a representative set of 996 genome sequences showing variant assignments and the locations of amino acid changes that increase (blue) or decrease (red) viral copies. (**B**) The temporal dynamics of the SNPs from February 2021 to March 2023. The transparency of the color corresponds to the mutation fraction in the daily sequence count: transparent color indicates low fractions, and opaque color indicates high fractions.

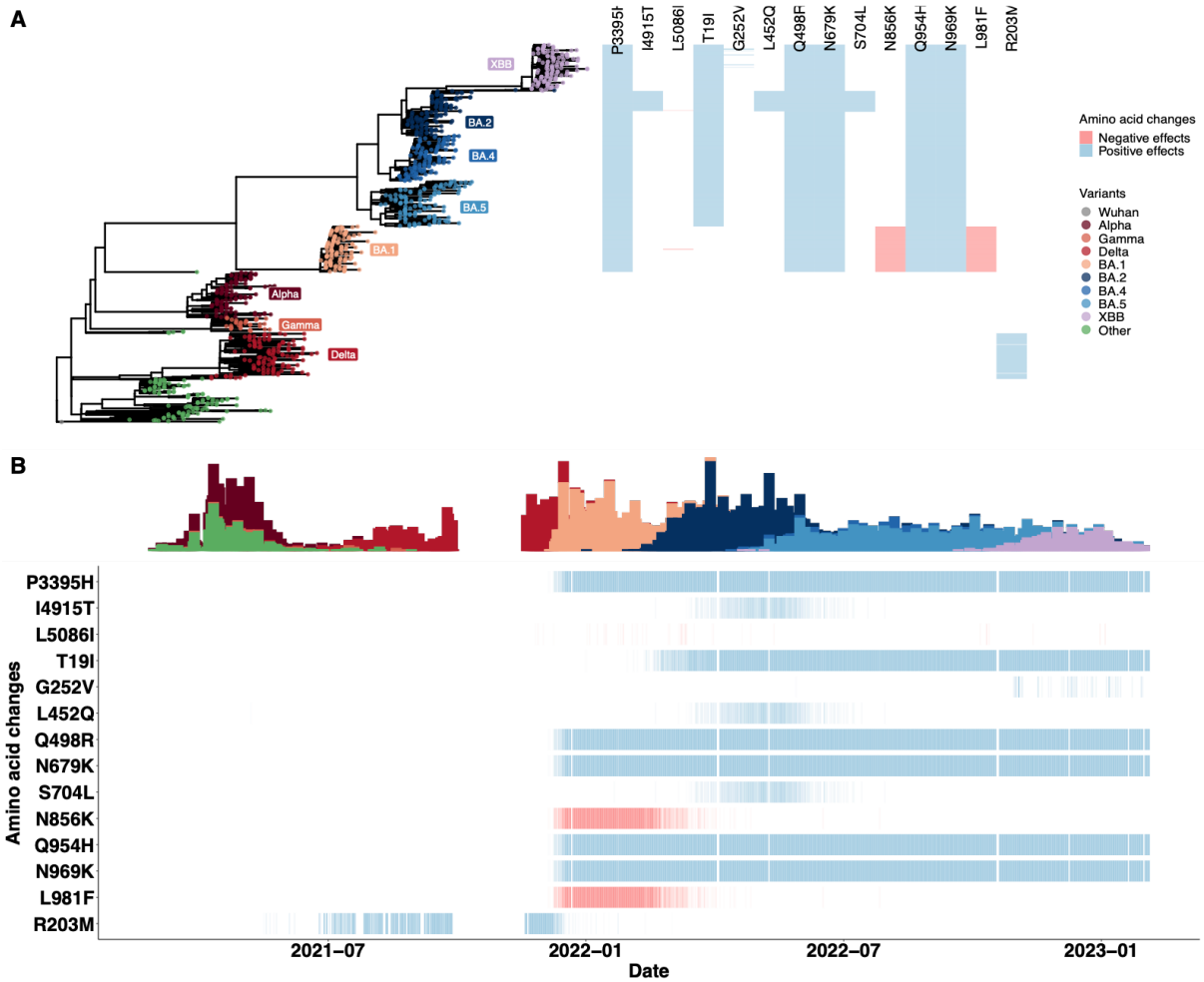

Supplemental Figure 9. The temporal dynamics of amino acid changes in the ORF1ab gene (P3395H, I4915T and L5086I), S gene (T19I, G252V, L452Q, Q498R, N679K, S704L, N856K, Q954H, N969K and L981F), and N gene (R203M) associated with changes in viral copies. The results are based on the multivariate regression analysis using the sequence clusters (i.e., a categorical variable) inferred from the MDS components, such that $Y \sim \alpha W + \beta_i SNP_i + \eta Cluster + e$. (**A**) The phylogenetic tree estimated from a representative set of 996 genome sequences showing variant assignments and the locations of amino acid changes that increase (blue) or decrease (red) viral copies. (**B**) The temporal dynamics of the SNPs from February 2021 to March 2023. The transparency of the color corresponds to the mutation fraction in the daily sequence count: transparent color indicates low fractions, and opaque color indicates high fractions.

AminoAcidChange	coefficients	Standard deviation
D3G	-0.5289821	0.06197068
T19R	-0.3583990	0.05236202
T19I	0.8675393	0.09368981
S26L	-0.3470353	0.05215769
T40I	-0.3810594	0.05035466
D63G	-0.3508300	0.05236169
A67V	-0.5034788	0.06039024
I82T	-0.3456858	0.05196310
S135R	0.8074352	0.09059436
V213G	0.2323215	0.03223704
T223I	0.5872878	0.08264916
G252V	1.1976598	0.12468634
S371L	-0.5534597	0.06193220
T376A	0.8620845	0.08999643
D405N	0.8797794	0.09241162
R408S	0.6207915	0.08287705
S413R	0.8157651	0.09230739
G446S	-0.2664795	0.03198609
L452Q	0.3466409	0.03292778
G496S	-0.5499511	0.06210286
T547K	-0.5341148	0.06147332
P681R	-0.3506782	0.05225140
S704L	0.3418159	0.03284982
T842I	0.7544330	0.08850513
N856K	-0.5521347	0.06227279
K856R	-0.5393076	0.06198051
D950N	-0.3534498	0.05196289
L981F	-0.5521347	0.06227279
A1306S	-0.3553043	0.05035843
G1307S	0.8259626	0.08905459

P2287S	-0.3541119	0.05015436
A2710T	-0.5450373	0.06223708
V2857A	-1.3198257	0.20083279
V2930L	-0.3796890	0.05042589
L3027F	0.8277260	0.08812009
T3090I	0.7634935	0.08992720
T3255I	-0.2507549	0.03705032
T3646A	-0.3687172	0.05037977
I3758V	-0.5466932	0.06187469
I4915T	0.3524137	0.03336264
L5086I	-1.2284741	0.13159986
S5150F	0.8465102	0.09162000
H5401Y	-0.3689352	0.05186462
K6597R	0.8501061	0.09021831

Supplemental Table 1. The identified amino acid changes associated estimated effective sizes and standard deviations using the multivariate linear regression model with MDS-computed dimensions as covariates.

AminoAcidChange	coefficients	Standard deviation
T19I	0.2123842	0.03172457
R203M	1.6492504	0.15825678
G252V	1.2301542	0.12381144
L452Q	0.3127277	0.03308999
Q498R	0.2123842	0.03172457
N679K	0.2123842	0.03172457
S704L	0.3077803	0.03301503
N856K	-0.2832514	0.03621949
Q954H	0.2123842	0.03172457
N969K	0.2123842	0.03172457
L981F	-0.2832514	0.03621949
P3395H	0.2123842	0.03172457
I4915T	0.3189265	0.03351622
L5086I	-1.1958547	0.13116867

Supplemental Table 2. The identified amino acid changes associated estimated effective sizes and standard deviations using the multivariate linear regression model with categorical clusters as covariates.